ISSN 1028-8546

Volume XXVII Number 3
Section: En October, 2021

Azerbaijan Journal of Physics

Fizika

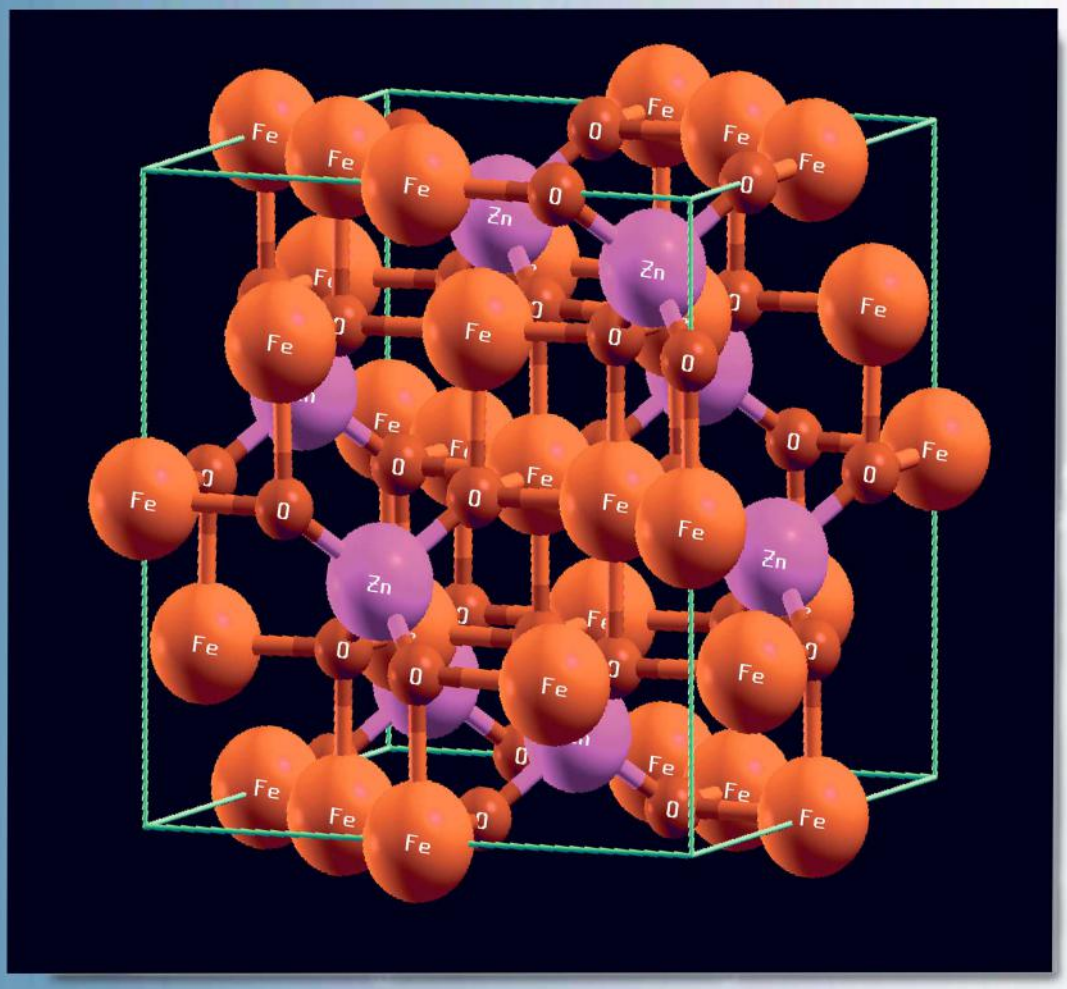

www.physics.gov.az
www.physics.gov.az/ajpfizika.html

Institute of Physics
Azerbaijan National Academy of Sciences
Department of Physical, Mathematical and Technical Sciences

Published from 1995
Ministry of Press and Information
of Azerbaijan Republic,
Registration number 514, 20.02.1995

ISSN 1028-8546
vol. XXVII, Number 03, 2021
Series: En

Azerbaijan Journal of Physics

FIZIKA

Institute of Physics
Azerbaijan National Academy of Sciences
Department of Physical, Mathematical and Technical Sciences

PUBLISHING OFFICE

131, H. Javid ave., AZ-1143, Baku
ANAS, Institute of Physics

Tel.: (99412) 539-51-63, 539-32-23
Fax: (99412) 537-22-92
E-mail: jophphysics@gmail.com
Internet: www.physics.gov.az

Published at "_____"
_____str., Baku

Sent for printing on: __.__. 201_
Printing approved on: __.__. 201_
Physical binding:_____
Number of copies:_____200
Order:_____

It is authorized for printing:

EFFECTS OF GEOMETRICAL SIZE ON THE INTERBAND LIGHT ABSORPT ION A QUANTUM DOT SUPERLATTICE

V.M. SALMANOV[1], B.G. IBRAGIMOV[2,3]
[1]Baku State University, AZ 1073/1 Baku, Azerbaijan
[2]Institute of Physics, Azerbaijan National Academy of Sciences,
[3]Azerbaijan State Oil and Industry University
Corresponding author: E-mail: Behbud.ibrahimov.93@mail.ru

We study in this paper the direct interband transitions in a quantum dot superlattice system. We obtain the analytical expressions for the light interband absorption coefficient and threshold frequency of absorption as the functions of geometrical size of quantum dot superlattice system. According to the results obtained from the present work, we find that the absorption threshold frequency decreases when the size of quantum dot superlattice increases.

Keywords: Absorption coefficient, interband transition, quantum wells, quantum wires, quantum dots, superlattices, quantum dot superlattice.
PACS: 78.55; 73.22.CD,7322

Over the last decades, there has been considerable interest in low-dimensional semiconductor systems in which the electron motion is strongly confined such as quantum wires, quantum dots, etc. Low-dimensional semiconductor structures include quantum wells, quantum wires, quantum dots, superlattices, and so on. Since in the systems one, two or three of the dimensions become of the order of the de Broglie wavelength for electrons, new quantum effects are expected [1].

Low-dimensional semiconductor structures, particularly quantum dots are attracting considerable attention recently, in part, because they exhibit novel physical properties and also with potential and real applications in many electronic and optoelectronic devices. In the last decades, a modern technologies, in particular such as Stranski-Krastanov epitaxial method have been developed to grow a wide variety of quantum dots structures having different geometries (spherical, parabolic, cylindrical and rectangular) and potentials (parabolic potential model, the square well model) [2-4].

Recent interest to semiconductor quantum dots is conditioned by new physical properties of these zero dimensional objects, which are conditioned by size-quantization effect of the charge carriers [5–7]. The presence of size quantization in all three directions makes the energy spectrum of charge carriers and strongly dependent on the geometry and linear dimensions of the sample [3]. It is clear that the more geometrical parameters characterize quantum dot, the more exibly one can control its energy spectrum. The subject of quantum dots as low- dimensional quantum systems has been the focus of extensive theoretical investigations. Much effort has recently been done in understanding their electronic, optical and magnetic properties.

In the last few yeas there has been considerable theoretical and experimental study has been carried out on the electronic and optical properties of multiple quantum well heterostructures. The central motivation of such studies has been the possible applications of these systems in optoelectronic devices. Growth techniques, such as molecular-beam epitaxial and metal- organic chemical vapor deposition, have made possible the fabrication of highly pure structures with abrupt interfaces, allowing for the tailoring of the electronic structure to suit almost any need. An interesting example is the variably spaced semiconductor superlattice [8].

Quantum dot superlattices are hence expected to display radically different non-equilibrium transport properties than quantum well superlatices. Potential applications for high performance thermoelectric converters [9], photovoltaics[10], and quantum cascade lasers [11] further motivates the fundamental understanding of the nonequilibrium transport properties of superlattices with 3D quantum confinement.

Quantum dot superlattice structures, which have a delta-function distribution of density of states and discrete energy levels due to three-dimensional quantum confinement, a potentially more favorable carrier scattering mechanism, and a much lower lattice thermal conductivity, provide the potential for better thermoelectric devices [12].

As we know, the study of the optical properties of low-dimensional semiconductor structures is important, not only to know, but also in the fabrication and subsequent working of electronic and optical devices based on such systems. There are many theoretical and experimental works on the optical properties of nanostructures such as quantum dots, quantum wires, and quantum wells [13-21]. The optical properties of low-dimensional semiconductor systems are especially useful in giving detailed information about their microscopic physics. One of the interesting optical properties is the light interband absorption coefficient. The spectroscopy of optical transitions across the band gap (interband transitions) is a powerful and versatile method to study the electronic structure of semiconductors. The optical properties of quantum dot for the first time were considered by Efros and Efros [4] at theoretical investigation of direct light absorption in spherical quantum dot with indefinitely high walls. Andreev and

131, H.Javid ave, AZ-1143, Baku
ANAS, Institute of Physics
E-mail: jophphysics@gmail.com

Lipovskii [22] discussed the influence of anisotropy of band structure on optical transitions in spherical quantum dots.

Even though considerable attention has been given to the study of the light interband absorption of the semiconductor quantum dots superlattice structures.

The light interband absorption of quantum dot superlattice structures has not been investigated so far. In the present work, we study the interband light absorption in a quantum dot superlattice structures. We obtain the light interband absorption coefficient and show dependencies of the absorption threshold frequency and on geometrical size of quantum dot superlattice structures**.**

The interband absorption in a quantum dot superlattice with a periodic potential U (z) of period d along the z-direction of the harmonic oscillator form is considered:

$$V(x,y)=\frac{m^*}{2}(\omega_x^2x^2+\omega_y^2y^2)\,, \qquad (1)$$

where m^* is the effective mass, ω_x *and* ω_y are the confinement frequencies in the x- and y-directions, respectively. Harmonic oscillator belongs to the most important and most commonly used physical models. Due to the formal simplicity, it is considered as one of the exactly solvable quantum mechanical problems. It is used to model a wide variety of phenomena ranging from molecular vibrations to the behaviour of quantized fields [23]. In the strong-coupling approximation, the Hamiltonian for charge carriers in a quantum dot superlattice can be written as [24, 25]:

$$H=\frac{(p_x^2+p_y^2)}{2m^*}+\frac{m^*}{2}(\omega_x^2x^2+\omega_y^2y^2)+\frac{\Delta}{2}(1-\cos\frac{p_zd}{\hbar})\ , \qquad (2)$$

where Δ is the miniband width. The electron effective mass $m^*=m_e$, when the conduction band is considered; and $m^*=m_h$ when the valence band is considered, where m_h is the effective mass of the hole.

The normalized eigenwave functions of the electron $\Psi_{n,e,k_z}(r)$ and the eigenvalues of the energy $E_{n,l}(k_z)$ in the conduction band are set, respectively, in the form [26]:

$$\Psi_{n,l,k_z}(r)=\frac{1}{\sqrt{L}_z}\Psi_n(x)\Psi_l(y)\xi_{k_z}(z)\ \ , \qquad (3)$$

$$E_{n,l}(k_z)=(n+\frac{1}{2})\hbar\omega_x+(l+\frac{1}{2})\hbar\omega_y+\frac{\Delta}{2}(1-\cos k_zd)=\varepsilon_{n,l}+\varepsilon(k_z)\ , \qquad (4)$$

where $n(=0,1,2,...)$ and $l(=0,1,2,...)$ are the level indices of the electronic subbands, k_z is the component of the wave vector in the z-direction, $\Psi_n(x)$, $\Psi_l(y)$ are the eigenwave functions of the harmonic oscillator, $H_n(x)$, $H_l(y)$ is the Hermite polynomial, $l_x=\sqrt{\hbar/(m^*\omega_x)}$, $l_y=\sqrt{\hbar/(m^*\omega_y)}$, $\xi_{k_z}(z)$ is the Bloch function in the approximation of strong coupling in the z-direction, and L_z is the normalized length in the direction.

The eigenwave functions of the harmonic oscillator for the conduction band are set,

$$\Psi_{n_e}\left(\frac{x}{l_{xe}}\right)=\sqrt{1/\sqrt{\pi}l_{xe}2^{n_e}n_e!}\exp\left[-x^2/2l_{xe}^2\right]H_{n_e}\left(\frac{x}{l_{xe}}\right) \qquad (5)$$

$$\psi_{l_e}\left(\frac{y}{l_{ye}}\right)=\sqrt{1/\sqrt{\pi l_{ye}}2^{l_e}l_e!}\exp\left[-y^2/2l_{ye}^2\right]H_{l_e}\left(\frac{y}{l_{ye}}\right) \qquad (6)$$

The eigenwave functions of the harmonic oscillator for the valence -band can be expressed as

$$\Psi_{n_h}\left(\frac{x}{l_{xh}}\right)=\sqrt{1/\sqrt{\pi}l_{xh}2^{n_h}n_h!}\exp\left[-x^2/2l_{xh}^2\right]H_{n_h}\left(\frac{x}{l_{xh}}\right) \qquad (7)$$

$$\psi_{l_h}\left(\frac{y}{l_{yh}}\right)=\sqrt{1/\sqrt{\pi}l_{yh}2^{l_h}l_h!}\exp\left[-y^2/2l_{yh}^2\right]H_{l_h}\left(\frac{y}{l_{yh}}\right) \qquad (8)$$

Expressions Eqs (3) - (8) show the charge carriers energy spectrum and wave functions in quantum dot superlattice system. These relations allow to calculate the direct interband light absorption coefficient in quantum dot superlattice system.

Since in the future we will consider transitions in the quantum dot superlattice, where instead of quasicontinuous bands of the energy spectrum we have a set of discrete energy values, it follows that after integration, we should proceed to summation over quantum numbers. As a result, the equation for the absorption coefficient of a quantum dot superlattice can be expressed by [4]:

$$K(\Omega) = A_0 \sum_{v,v'} \left| \int_V \psi_v^e \psi_{v'}^h dV \right|^2 \delta\left[\hbar\Omega - E_g - E_v^e - E_{v'}^h\right] \tag{9}$$

where A_0 is the quantity proportional to the square of dipole moment matrix element modulus, taken on Bloch functions.

The $\sum_{v,v'} \left| \int_V \psi_v^e \psi_{v'}^h dV \right|^2$ can be obtained using following expressions

$$J_{n_e n_h} = \int_{-\infty}^{\infty} \Psi_{ne}\left(\frac{x_e}{l_{ye}}\right) \Psi_{nh}\left(\frac{x_h}{l_{yh}}\right) dx \tag{10}$$

$$J_{l_e l_h} = \int_{-\infty}^{\infty} \Psi_{le}\left(\frac{y_e}{l_{ye}}\right) \Psi_{lh}\left(\frac{y_h}{l_{yh}}\right) dy \tag{11}$$

where $J_{n_e n_h}$ and $J_{l_e l_h}$ are overlap integrals between the valence and conduction bands.

From Eqs.(9)-(10) it follows that quantum numbers n_e, n can change arbitrarily. The argument of the Dirac δ-function allows to define the threshold frequency of absorption Ω_{00}.

CONCLUSION

In this work, we have studied the direct interband transitions quantum dot superlattice. We obtained the analytical expressions for the light interband absorption coefficient and threshold frequency of absorption geometrical size of quantum dot superlattice. We studied the dependence of absorption threshold frequency on quantum dot superlattice size. According to the results obtained from the present work, it is deduced that the quantum dot superlattice size play important roles in the absorption threshold frequency.

[1] *M.J. Kearny and P.N. Butcher.* Journal of Physics C: Solid State Physics, 1987, Volume 20, Number 147.

[2] *Z.I. Alferov.* Semiconductors. The history and future of semiconductor heterostructures, Fiz. Tekh. Poluprovodn. 32, 1–18 (January 1998).

[3] *D.D. Bimberg, M. Grundmann, and N.N. Ledentsov*. Quantum Dot Heterostructures, Wiley, Chichester, 1999.

[4] *A.L. Efros and A.L. Efros.* "Interband absorption of light in a semiconductor sphere", Semiconductors 16 (7), 772–775, 1982.

[5] *P. Harrison, Quantum Wells, Wires and Dots*. Theoretical and Computational Physics (John Wiley & Sons Ltd, NY, 2005).

[6] *G. Bastard.* Wave Mechanics Applied to Semiconductor Heterostructures (Les editions de physique, Les Ulis Cedex, Paris, 1989).

[7] *M. Bayer, O. Stern, P. Hawrylak, S. Fafard, A. Forchel*. Hidden symmetries in the energy levels of excitonic 'artificial atoms', 2000, Nature 405, 923.

[8] *J.N. Zuleta, E. Reyes-Gómez.* Eects of crossed electric and magnetic fields on the interband optical abffsorption spectra of variably spaced semiconductor superlattices. Physica B 2016, http://dx.doi.org/10.1016/j.physb.2016.02.011i

[9] *Y.M. Lin and M.S. Dresselhaus.* Thermoelectric properties of superlattice nanowires, Phys. Rev. B 68, 075304, 2003.

[10] *A. Nozik.* Quantum dot solar cells, Physica E 14, 115, 2002.

[11] *N. Wingreen and C. Stafford*. Quantum-dot cascade laser: proposal for an ultralow-threshold semiconductor laser, IEEE J. Quantum Electron. 33, 1170, 1997.

[12] *T.C. Harman, P.J. Taylor, M.P. Walsh, B.E. La.* Forge Quantum Dot Superlattice Thermoelectric Materials and Devices. *Science* 297, 2002, p. 2229-2232.

[13] *R. Khordad* Effects of magnetic field and geometrical size on the interband light absorption in a quantum pseudodot system Solid State Sciences 12, 2010, 1253-1256.

[14] *G.B. Ibragimov*. Free - Carrier Absorption in Quantum Well Structures for Alloy - Disorder Scattering Physica Status Solidi B v.231, Issue2 June 2002 Pp. 589-594.

[15] *G.B. Ibragimov*. Interface roughness induced intrasubband scattering in a quantum well under an electric field Semiconductor Physics Quantum Electronics & Optoelectronics, 2002, tom 5, № 1. — С. 39-41.

[16] *V.V. Karpunin, V.A. Margulis.* Absorption of the electromagnetic radiation in quantum wire with a anisotropic parabolic potential placed in the

transverse magnetic field. FTP 50, 6, 2016, pp. 785-790.

[17] *A.V. Shorokhov, V.A. Margulis*. Intraband resonance scattering of electromagnetic radiation in anisotropic quantum dots. Nanosystems: Physics, Chemistry, Mathematics, 2010, 1, 1, 178–187.

[18] *D.Q. Khoa, N.N. Hieu, T.N. Bich, Le T.T. Phuong, B.D. Hoi, Tran P.T. Linh, Quach K. Quang, C.V. Nguyen, H.V. Phuc.* Magneto-optical absorption in quantum dot via two-photon absorption process. Optik, 2018, v. 173, 263-270.

[19] *V. Lozovski and V. Piatnytsia*. "The analytical study of electronic and optical properties of pyramid-like and cone-like quantum dots," J. Comput. Theor. Nanosci. 2011, 8(11), 2335–2343.

[20] *F.M. Hashimzade, T.G. Ismailov, B.H. Mehdiyev and S.T. Pavlov*. Interband electron Raman scattering in a quantum wire in a transverse magnetic field Phys.Rev. 2005, B 71, 165331.

[21] *F.M. Peeters.* "Magneto-optics in parabolic quantum dots," Phys. Rev. B 42(2), 1990, 1486–1487.

[22] *A.D. Andreev, A.A. Lipovskii*. Effect of anisotropy of band structure on optical gain in spherical quantum dots based on PbS and PbSe, Semiconductors 33(12), 1999, 1304–1308.

[23] *Sameer M. Ikhdair, Majid Hamzavi, Ramazan Sever.* Spectra of cylindrical quantum dots:The effect of electrical and magnetic fields together with AB flux field. Physica B 407 (2012) 4523–4529.

[24] *W.M. Shu and X.L. Lei*. Miniband transport in semiconductor superlattices in a quantized magnetic field. Phys. Rev. B 50, 1994, 17378.

[25] *S.C. Lee, D.S. Kang, J.D. Ko, Y.H. Yu, J.Y. Ryu and S.W. Kim.* Magnetophonon Resonances in the Miniband Transport in Semiconductor Superlattices J. Korean, Phys. Soc. 39, 2001, 643.

[26] *S.C. Lee.* Electrophonon Resonance in Quantum-Dot Superlattices J. of Korean Phys. Soc, 52, 2008, 1081.

Received: 24.06.2021

RAMAN SCATTERING OF InSb-CrSb, InSb-Sb, GaSb-CrSb EUTECTIC COMPOSITES

M.V. KAZIMOV
Institute of Physics of Azerbaijan National Academy of Sciences
AZ 1143, Baku, H.Javid ave., 131
E-mail: **mobilkazimov@gmail.com**

Semiconductor-metal İnSb-CrSb, İnSb-Sb, GaSb-CrSb eutectic composites are synthesized by the vertical Bridgman method. The interphase zones around metallic inclusions in GaSb-CrSb, InSb-CrSb and InSb-Sb eutectic composites have been revealed by study of the structure and elemental composition. It has been found that the peaks detected in the Raman spectra correspond to the GaSb and InSb compounds and Sb-Sb bond.

Keywords: Eutectic composite, Raman Scattering; SEM structure, X-ray diffraction
PACS: 539.24/27

1. INTRODUCTION

One of the main features of eutectic composites obtained based on InSb, GaSb and 3d-transition elements is the anisotropy in kinetic coefficients depending on the direction of metal needles [1-5]. These composites, which combines both semiconductor and metallic properties, behave as nonhomogeneous semiconductors since metal needles are distributed parallel to the crystallization direction. The composites formed by the 3d-transition metals are considered to be diluted magnetic semiconductors. Recently, NiAs-type hexagonal structure CrSb has been widely studied as a suitable material for spintronics [6-10]. According to the results of these studies, the connection between the ferromagnetic constituents perpendicular to the crystallization axis in the CrSb junction is antiferromagnetic. Consequently consideration of the InSb-CrSb, InSb-Sb and GaSb-CrSb systems is of substantial interestl. The present paper is devoted to synthesis, structure and Raman scattering investigated of InSb-CrSb, InSb-Sb and GaSb-CrSb eutectic composites.

2. EXPERIMENTAL DETAILS

2.1 Synthesis

In order to synthesize InSb-CrSb, InSb-Sb, and GaSb-CrSb eutectic composites, InSb and GaSb are first synthesized: the stoichiometric quantities of In and Sb, Ga and Sb are melted together and treated with horizontal zone alloy.The velocity along the melting zone crystallization was 12mm/h.; the concentration of carriers in InSb and GaSb compounds was $n=2x10^{16}$ and $p=1.8x10^{17}$ at room temperature, respectively.

Eutectics with the following mixtures: InSb and 0.6% CrSb for InSb-CrSb, InSb and 37.3% Sb for InSb-Sb, GaSb and 13.4% CrSb for GaSb-CrSb systems were filled into quartz ampoules at a pressure of 10^{-2} Pa.The ampoules were stored in an electric oven at 1200K for 4 hours and cooled to room temperature. At the next stage, InSb-CrSb, InSb-Sb and GaSb-CrSb composite crystallization is carried out by the vertical Bridgman method with different crystallization rates: 1.2mm/min.; 0.6mm/min. and 0.3mm/min. at temperature gradient 20-30K [5].

2.2 Caracterization

The X-ray spectra of the InSb-CrSb, InSb-Sb and GaSb-CrSb composites were made by the Advance-D8 diffractometer ("Bruker"). The source of radiation was the CuKα-anode, operating at a voltage of 40kV and a current of 40 mA. The wavelength of the radiation was λ=1.5406Å, and the angle between the falling X-rays and the sample was 2Θ=5÷80. Microstructure analysis was performed on surface of the samples parallel and perpendicular to crystallization directions by the Zeiss Sigma ™ Field Emission, SEM-Scanning Electron Microscope.

3. DISCUSSION

Diffraction patterns of GaSb-CrSb eutectic composite are shown in Fig. 1. Analysis of XRD spectra confirmed that this system is diphasic: the most intense peaks corresponding to the (111), (200), (220), (311), (222), (400), (331), (420), and (422) Muller index are identical to the GaSb matrix, while the weak peaks found at 2θ=30º, 44.08º, 52.12º, and 54.13º coincide with the CrSb lines having a hexogonal structure with lattice parameters of a=4.121, c=5.467, c/a=1.327, and the P63/mmc space group.

Fig. 2 shows the diffraction patterns of the InSb-CrSb eutectic composite. The most intense peaks corresponding to the (111), (220), (311), (400), (311), (422) və (511) Muller index are identical to the InSb matrix, while the weak peaks found at 2θ=30º, 44.08º, 52.12º, and 54.13º coincide with the CrSb line.

Fig. 3 shows the diffraction patterns of the InSb-Sb eutectic composite. The most intense peaks corresponding to the (111), (220), (311), (400), (311), (422) və (511) Muller index are identical to the InSb matrix, while the weak peaks found at 2θ=30º, 44.08º, 52.12º, and 54.13º coincide with the CrSb line.

Shown in Fig. 4 the structure of the films is it can be seen structural formations of a round shape are evenly distributed on the surface of the film.

131, H.Javid ave, AZ-1143, Baku
ANAS, Institute of Physics
E-mail: jophphysics@gmail.com

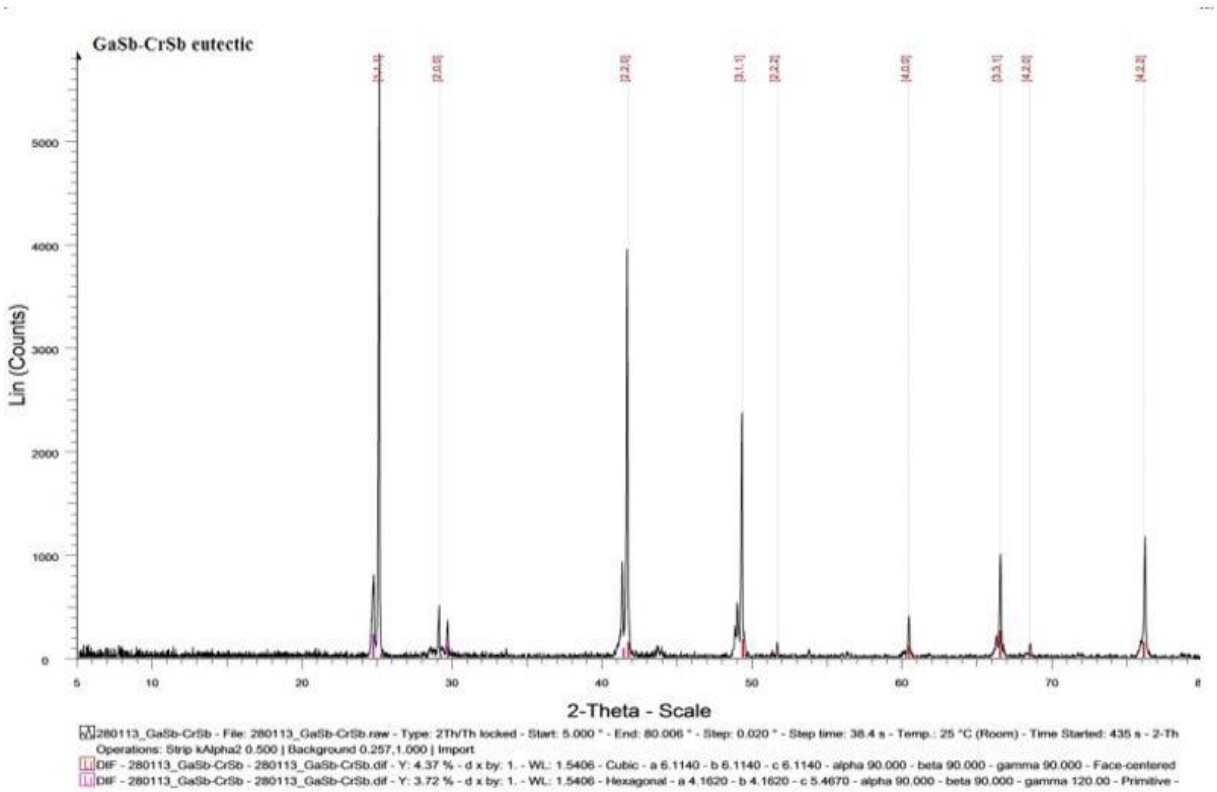

Fig. 1. X-ray spectrum of GaSb-CrSb eutectic composite.

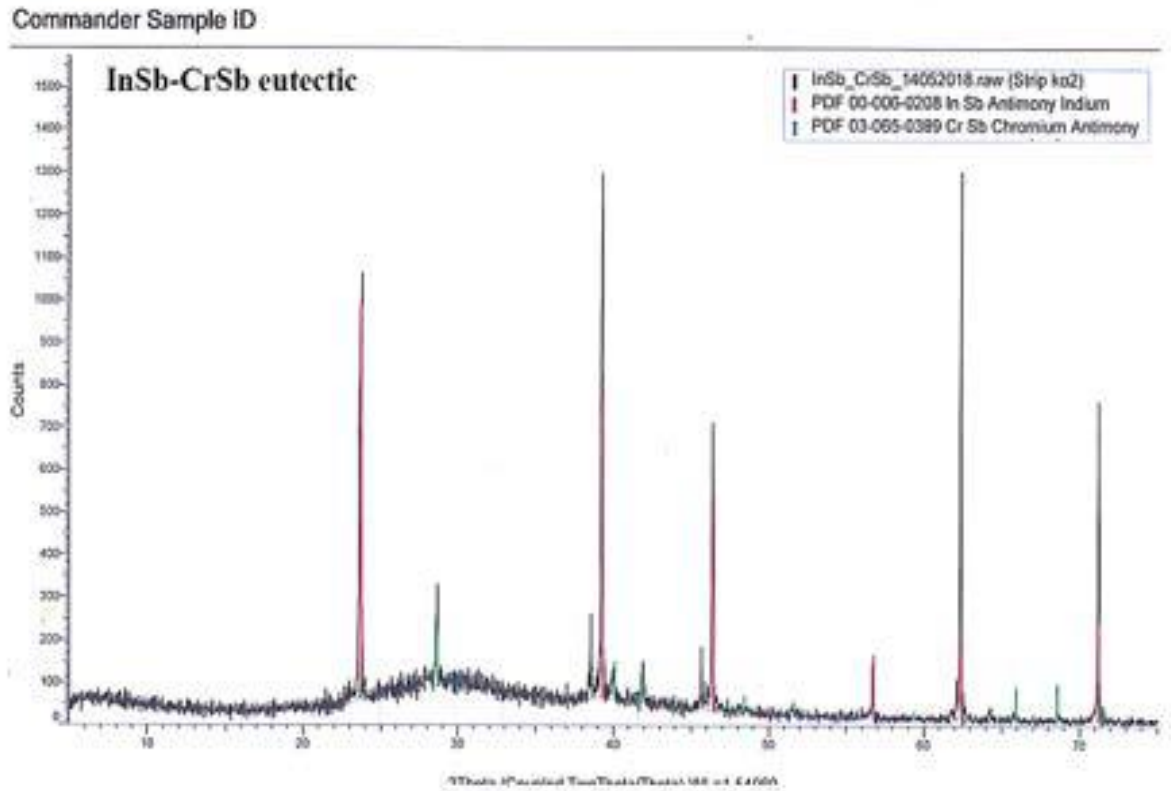

Fig. 2. X-ray spectrum of InSb-CrSb eutectic composite

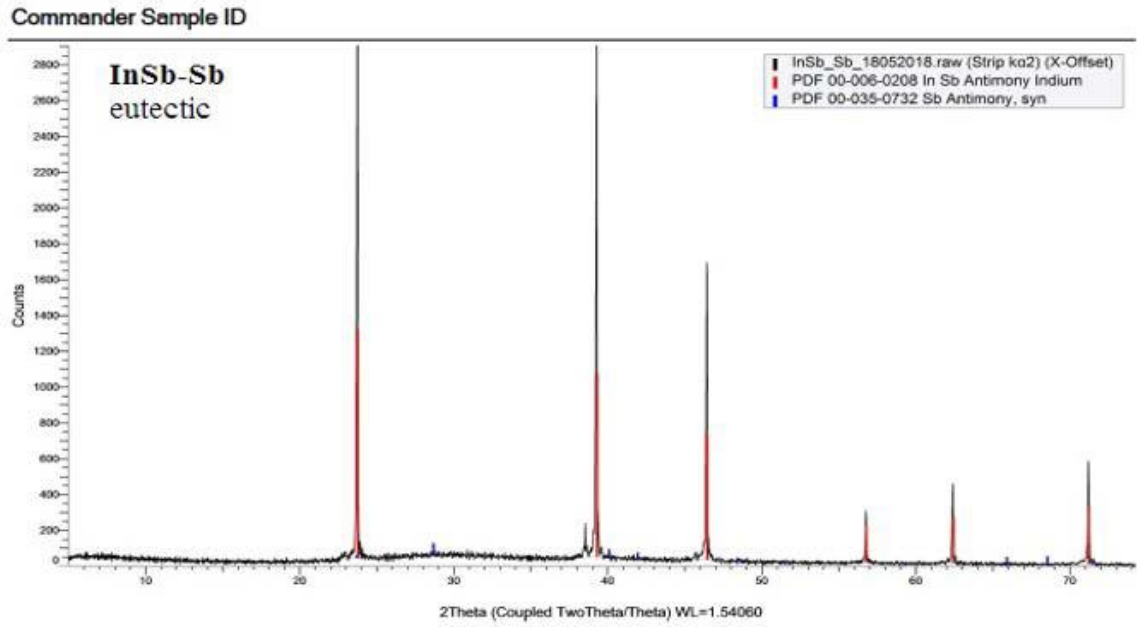

Fig. 3. X-ray spectrum of InSb-Sb eutectic composite

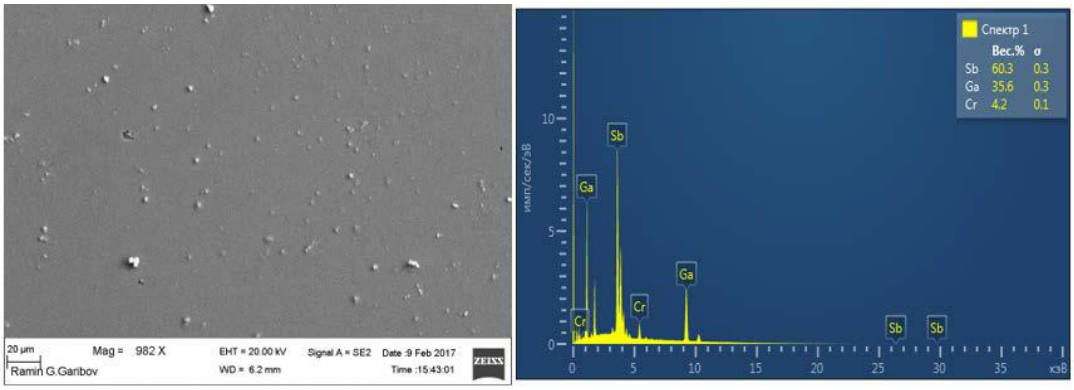

Fig. 4. X-ray spectra of GaSb–CrSb thin film obtained with SEM–EDX

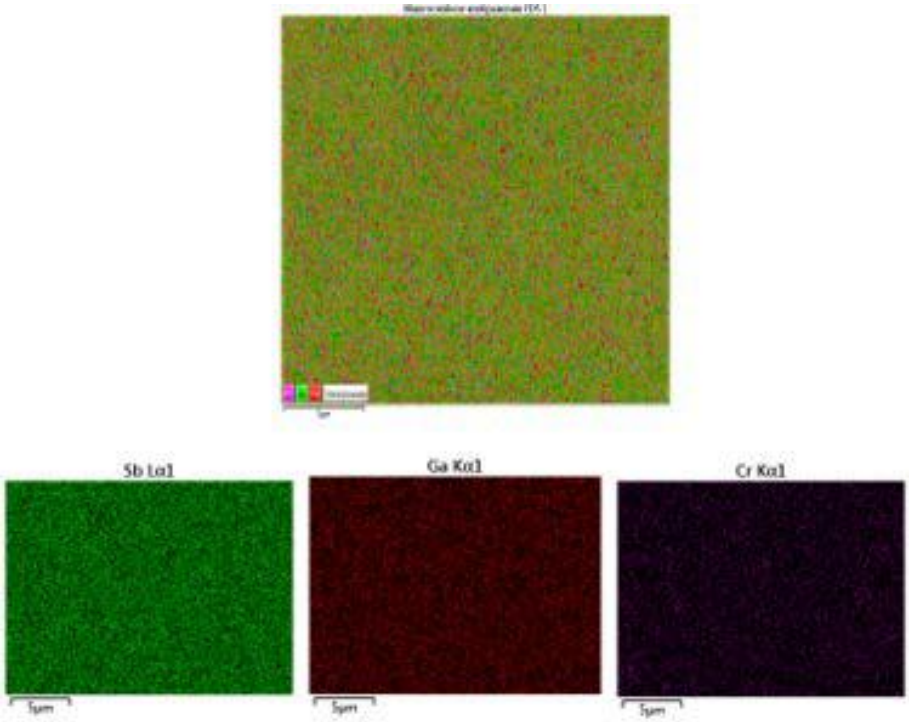

Fig. 5. Element map of the GaSb–CrSb composite

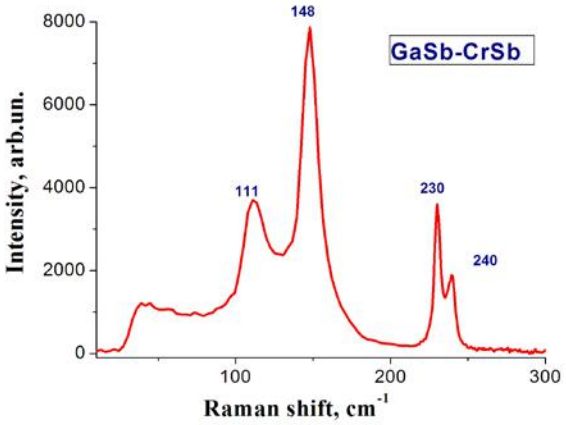

Fig. 6. Raman spectra of GaSb-CrSb eutectic composite.

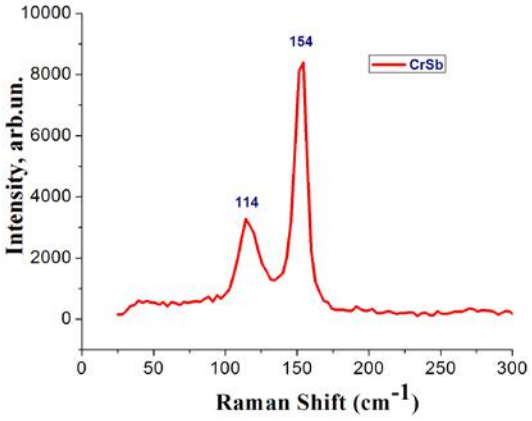

Fig. 7. Raman spectra of CrSb compound

The length of the metal rods (1-1.6 μm in diameter) is 10-100μm in InSb-CrSb composite, 30-50 μm in GaSb-CrSb, 40-100μm in InSb-CrSb. As it is seen from Fig. 4, the metal rods are evenly distributed in the matrix in the direction of crystallization. Fig.5 shows an element map of the GaSb-CrSb eutectic alloy. In the specific map, the colours red, blue and green indicate Sb (L), Cr (K) and Ga (K), respectively and black colour indicates the absence of this element.

Raman analysis is an important tool to study atomic interactions in semiconductors and the dynamics of the crystal lattice [12-15].Raman analysis were investigated to confirm the existence of two-phase and inter-phase zones in the GaSb-CrSb, InSb-CrSb, InSb-Sb eutectic composites at room temperature. Fig.7 and Fig.8 shows the Raman lines at about 111cm^{-1}, 148cm^{-1}, 230cm^{-1}, 240cm^{-1} are the mode LO GaSb-CrSb eutectic composite, and 114cm^{-1}, 154cm^{-1}, 240cm^{-1} for CrSb compound.

Some parameters of semiconductor-metal type InSb-CrSb, InSb-Sb, and GaSb-CrSb eutectic composites are shown in the table [1, 4, 5].

Fig.8 (a) and (b) are shows the Raman lines about InSb-CrSb composite are 101cm^{-1}, 145cm^{-1}, 174cm^{-1} and (b), respectively, at 101cm^{-1},150cm^{-1} and 240cm-$^{-1}$.

Thus, X-phase analysis of InSb-CrSb, GaSb-CrSb and InSb-Sb alloys is a composite composite comprising matrix (InSb and GaSb) and porous metal coatings (CrSb and Sb) based on studies in optical and electron microscopes. The Raman spectra obtained in the InSb-CrSb and GaSb-CrSb compositions only characterize the Sb-Sb bond [13,15].

Eutectic composites	Metal phase weight %	Needles density, mm^{-2}	Needles diameter, μm	Needles length, μm	Crystallization speed, mm/min	Concentration, cm^{-3}
InSb-CrSb	0,6	0,6x10^4	1	100-200	1,2	p=2x10^{17}
InSb-Sb	37,6	2,5x10^4	1,6	40-100	1,4	p= 10^{17}
GaSb-CrSb	13,4	5,2x10^4	1,4	30-50	0,3-0,6	p=8x10^{17}

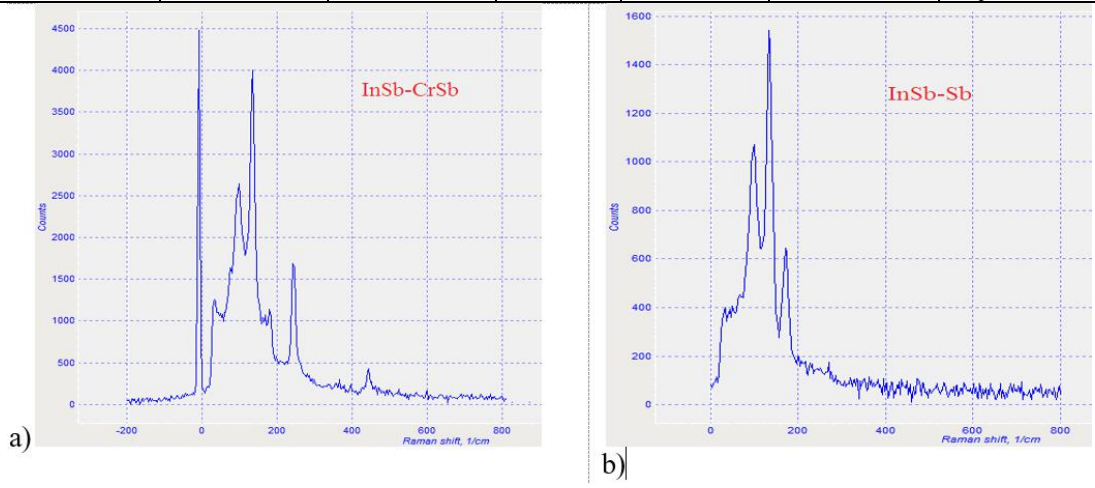

Fig. 8. Raman spectra of InSb-CrSb (a) and InSb-Sb (b) eutectic composites

[1] *M. V. Kazimov, D. H. Arasly, R. N. Rahimov, A. A. Khalilova, I. K. Mammadov.* Magnetic and electrical properties of GaSb-CrSb eutectic system, Journal of Non-Oxide Glasses, 5(1), pp. 7–11, 2020.

[2] *Y. Umehara, S. Koda.* Structure of a unidirectionally solidified GaSb-CrSb eutectic alloy // J.Japan İnst. Metals, v.50, pp.666-670, 1986.

[3] *J.A. Graves.* Undercooling and Solidification Behavior in the InSb-Sb System, NASA CR-175013, pp.216, September 1985,

[4] *M. V. Kazimov, D. H. Arasly, I. Kh. Mammadov, R. N. Rahimov, A. A. Khalilova.* Influence of inter-facial phases on thermal and electrical conductivity in GaSb-CrSb eutectic system, Azerbaijan Journal of Physics, 24 (3), pp.29-32, 2018.

[5] *R. N. Rahimov, M. V. Kazimov, D. H. Arasly, A. A. Khalilova, I. Kh. Mammadov*. Features of Thermal and Electrical Properties of GaSb-CrCb eutectic composite, Journal Ovonic Research, 13(3), pp.113 – 118, 2017.

[6] *Liu Yong, S.K. Bose, J. Kudrnovsky.* Magnetism and half-metallicity of some Cr-based alloys and their potential for application in spintronic devices.World Journal of Engineering, 125-132, 9 (2012).

[7] *S. Polesya, G. Kuhn, S.Mankovsky, H. Ebert, M. Regus, W. Bensch.* Structural and magnetic properties of CrSb compound s: NiAs structure., J Phys Condens Matter. 24(3), 2012.

[8] *M. Shirai.* Possible half-metallic ferromagnetism in zinc blende CrSb and CrAs. J. Appl. Phys., 93(10), 2003.

[9] CrSb, physical properties, Springer & Material Phases Data System (MPDS), Switzerland & National Institute for Materials Science (NIMS), 2013.

[10] *N. Wang, Y. Cai, R.Q. Zhang.* Growth of NWs. Materials Science Engineering: Review Reports 60(1-6): 1-51. 2008.

[11] *F. M. Liu* et al. Raman properties of GaSb nanoparticles embedded in SiO_2 Films, Submitted to Journal of Physics: Condensed Matter, 2001.

[12] *C.E.M. Campos, P.S. Pizani.* Strain effects on As and Sb segregates immersed in annealed GaAs and GaSb by Raman spectroscopy, Journal of Applied Physics, 89 (2001) 3631-3633.

[13] *S. Winnerl, S. Sinning, T. Dekorsy, M. Helm.* Increased terahertz emission from thermally treated GaSb, Applied Physics Letters, 85 (2004) 30923094.

[14] *M. R. Joya, P. S. Pizania, R. G. Jasinevicius.* Raman scattering investigation on structural and chemical disorder generated by laser ablation and mechanical microindentations of InSb single crystal, J. Appl. Phys. 100, (2006) 053518

Received: 02.07.2021

DETERMINATION OF FREQUENCY IN TWO VALLEY SEMICONDUCTORS SUCH AS GaAs

E.R. HASANOV[1,2], Sh.G. KHALILOVA[2], R.K. MUSTAFAYEVA[1]

[1]Baku State Uviversity Acad. Z.Khalilov, str.23, Baku, Azerbaijan Republic
[2]Institute of Physics, ANAS, AZ-1143, H. Javid 131, Baku, Azerbaijan Republic,
shahlaganbarova@gmail.com

It is shown that the dimensions of the crystal play an essential role in the excitation of an unstable wave with a certain frequency and growth rate, and it is possible to regulate the appearance of current oscillations with a magnetic field. The values of the frequency of the current oscillation are found. The value of the external electric field and the frequency of current oscillation are determined at the initial point.

Keywords: instability, oscillations, growth rate, frequency, radiation.
PACS: 72.70.m, 72.70.+m, 73.40.Gk, 73.40.Jn, 73.40.Mr, 73.43.Jn.

INTRODUCTION

A simple way to convert electromagnetic energy using semiconductors that do not contain any electron-hole junctions is the phenomenon of electrical instability. The current-voltage characteristic (CVC) of such a sample is linear. Generation and amplification of electromagnetic oscillations, current stabilization, "memory" effect, etc. are possible. Instability depends on the characteristics of the solid. For example, in a GaAs crystal, the I–V characteristics and the energy spectrum of charge carriers are described by the following graphs

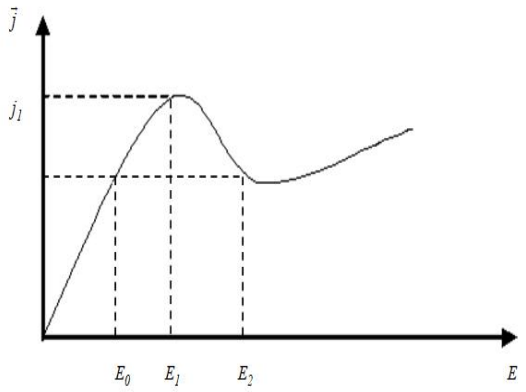

Fig. The dependence of the current density on the electric field is an N-shaped volt-ampere characteristic.

Field strength is a multivalued function of current density. The energy spectrum of electronic gallium arsenide is two-valley. With the help of an electric field, charge carriers are heated in the sub-zone with high mobility, as a result, having acquired a sufficiently high energy, they pass into the sub-zone with higher energy and low mobility.

The effective mass of charge carriers in GaAs are important $m_a = 0{,}072m_0$ $m_b = 1{,}2m_0$, and the mobility of charge carriers in the valleys are $\mu_a = \frac{e\tau}{m_a}$ and $\mu_b = \frac{e\tau}{m_b}$ ($\mu_a \ll \mu_b$, μ is the mobility of charge carriers). We will designate valleys 1-a, 2-b.

The total current has the form

$$\vec{j} = en_a\mu_a E + en_b\mu_b E = en\mu(E)E \quad (1)$$

$$n = n_a + n_b = const \ \frac{dn}{dt} = 0 \quad (2)$$

Instability in GaAs in 1963 was discovered experimentally by the English physicist J. Gann [1]. In theoretical works [2-3], the Gunn effect is investigated in the presence of an external electric field. All theoretical studies are calculated without carrier diffusion. However, in the scientific literature there are no theoretical works devoted to theoretical studies of the Gunn effect taking into account intervalley scattering based on the solution of the Boltzmann kinetic equation. In this theoretical work, we will calculate the frequencies of current oscillations in the presence of a strong magnetic field by applying the Boltzmann equation, taking into account the intervalley scattering of charge carriers.

$$\mu H_0 >> c \quad (3)$$

(H_0 is intensity of a constant magnetic field, c is speed of light)

THEORY

In a stationary state, the electric field is independent of time. Under the influence of an electric field for the current to be stationary, electrons must be scattered on any lattice inhomogeneities (vibrations of atoms or crystal defects). Under the action of external forces, the state of charge carriers cannot be described by the equilibrium distribution function $f_0(\varepsilon)$, but it is necessary to introduce a nonequilibrium distribution function $f(\vec{k},\vec{r})$, which is the probability that an

131, H.Javid ave, AZ-1143, Baku
ANAS, Institute of Physics
E-mail: jophphysics@gmail.com

electron with a wave vector (quasimomentum $\hbar\vec{k}$) is near a point. The distribution function $f(\vec{k},\vec{r})$ is found from the kinetic Boltzmann equation. It is assumed that the distribution function can change under the influence of two reasons, either under the influence of external factors, or under the influence of collisions of electrons with lattice vibrations (phonons) and crystal defects.

Then, in the considered stationary state, these factors compensate each other.

$$\left(\frac{\partial f}{\partial t}\right)_{external} + \left(\frac{\partial f}{\partial t}\right)_{collision} = 0 \qquad (4)$$

In the presence of external electric and magnetic fields, equation (4) has the form

$$\vec{V}\vec{\nabla} f + \frac{e}{\hbar}\left(E + \frac{1}{c}\left[\vec{V}\vec{H}\right]\right)\vec{\nabla}_{\vec{k}} f = \left(\frac{\partial f}{\partial t}\right)_{collision} \qquad (5)$$

$$\vec{V} = \frac{1}{\hbar}\nabla_{\vec{k}}\varepsilon(\vec{k})$$

Neglecting the anisotropic one, we solve the equation. We assume that for valley “a” with intravalley, and for valley “b”, intravalley scattering prevails over intervalley one. Then the Boltzmann equations for the valley "a" and "b" can be written in the following form

$$\left(\frac{\partial f^a}{\partial t}\right)_{external} + \left(\frac{\partial f^a}{\partial t}\right)_{intravalley} = 0 \qquad (6)$$

$$\left(\frac{\partial f^b}{\partial t}\right)_{внеш} + \left(\frac{\partial f^b}{\partial t}\right)_{внутридол} = 0 \qquad (7)$$

In [2] Davydov showed that in a strong electric field the distribution function can be represented in the form

$$f = f_0 + \frac{\vec{P}}{p}\vec{f}_1 \qquad (8)$$

($\vec{P}$ -momentum)

Then for the valleys “a” and “b” we write

$$f^a = f_0^a + \frac{\vec{P}}{p}\vec{f}_1^a,\ \ f^b = f_0^b + \frac{\vec{P}}{p}\vec{f}_1^b \qquad (9)$$

In [3], from solution (9), the distribution function f^b was found in the presence of an electric field

$$f_0^b = Be^{-\alpha_b(\varepsilon-\Delta)^2} \qquad (10)$$

$$f_1^b = -\frac{em_b l_b}{p}\vec{E}\frac{\partial f_0^b}{\partial p} \qquad (11)$$

Here

$$l_b = \frac{\pi\hbar^4\rho u_0^2}{D^2 m_b^2 k_0 T},\ \alpha_b = \frac{3D^4 m_b^5 k_0 T}{e^2\pi^2\hbar^8\rho^2 u_0^2 E^2} \qquad (12)$$

l_b - the length of the free path in the valley «b», D - deformation potential, T- grate temperature,

p -the density of the substance, u_0 - sound speed.

It was shown in [2] that in strong electric and magnetic fields in the case of intravalley scattering, the function f_1^b has the form:

$$f_1^b = -\frac{el_b m_b}{p}\frac{\partial f_0^b}{\partial p}\cdot\frac{\vec{E}+\frac{el_b}{cp}[\vec{E}\vec{H}]+\left(\frac{el_b}{cp}\right)^2\vec{H}(\vec{E}\vec{H})}{1+\left(\frac{el_b H}{cp}\right)^2} \qquad (13)$$

$$f_0^b = Be^{-\alpha_b(\varepsilon-\Delta)^2} \qquad (14)$$

(B -normalization constant)

$$\alpha_b = \frac{3D^4 m_b^5 k_0 T\left[1+\left(\frac{el_b H}{cp}\right)^2\right]}{e^2\pi^2\hbar^8\rho^2 u_0^2\left[E^2+\left(\frac{el_b}{cp}\right)^2(\vec{E}\vec{H})^2\right]} \qquad (15)$$

$$f_0^a = Ae^{-\alpha_a\varepsilon^2} \qquad (16)$$

We calculate the total current density

$$\vec{J} = \vec{j}_a + \vec{j}_b \qquad (17)$$

$$\vec{j}_a = \frac{e}{3\pi^2\hbar^3 m_a}\int_0^\infty f_1^a p^3 dp = \frac{e^2 l_a\alpha_a A}{3\pi^2\hbar^3 m_a^2}\left\{\vec{E}\left(\frac{cH}{el_a}\right)^2 p^7 e^{-\frac{\alpha_a p^4}{4m_a^2}}dp + \right.$$
$$\left. + \frac{el_a}{c}\left(\frac{cp}{el_a H}\right)^2\int_0^\infty p^6 e^{-\frac{\alpha_a p^4}{4m_a^2}}dp\left[\vec{E}\vec{H}\right] + \left(\frac{el_a}{c}\right)^2\left(\frac{cpH}{el_a}\right)^2\int_0^\infty p^5 e^{-\frac{\alpha_a p^4}{4m_a^2}}dp\vec{H}\left(\vec{E}\vec{H}\right)\right\} \qquad (18)$$

It can be written in $\vec{j}_b$ a similar way, only it is necessary to replace the index "a" with "b" and A with B. The integrals in (18) are calculated by the following formula (gamma function).

$$\int_0^\infty x^n e^{-x}dx = \Gamma(n+1) \qquad (19)$$

Applying formulas (19), we obtain expressions for the total current density of the expression

$$\vec{j} = \Sigma\vec{E} + \Sigma_1\left[\vec{E}\vec{h}\right] + \Sigma_2\vec{h}\left(\vec{E}\vec{h}\right) \qquad (20)$$

$$\Sigma = \frac{8nc^2 m_a^{1/2}\alpha_a^{-1/4}}{3\sqrt{2}l_a\Gamma(3/4)}\cdot\frac{1}{H^2}\cdot\left(\frac{m_b}{m_a}\right)^3\left(\frac{m_0}{m_a}\right)^{1/2}$$

$$\Sigma_1 = \frac{4enc}{H}\frac{\Gamma(7/4)}{\Gamma(3/4)} \quad (21)$$

$$\Sigma_2 = \frac{4e^2 nl_a\alpha_a^{1/4}}{3\sqrt{2}m_a^{1/2}}\cdot\frac{\Gamma(3/2)}{\Gamma(3/4)}\cdot\left(\frac{m_b}{m_0}\right)^{1/2}$$

After calculating (Σ,Σ_1,Σ_2), the frequencies of the current oscillation can be calculated. In work [4-5], we calculate the frequency of the current oscillation in the presence of a weak magnetic field ($\mu H >> c$)

To calculate the oscillation frequency, we find from Maxwell's equation the current density

$$\vec{j}' = \frac{c}{4\pi}rot\vec{H}' + \frac{1}{4\pi}\frac{\partial\vec{E}'}{\partial t} \quad (22)$$

and we will equate the expressions of currents (19-22), as a result we will receive the following expressions

$$\frac{c}{4\pi}rot\vec{H}' + \frac{1}{4\pi}\frac{\partial E'}{\partial t} = \Sigma\vec{E} + \Sigma_1\left[\vec{E}\vec{h}\right] + \Sigma_2\vec{h}\left(\vec{E}\vec{h}\right) \quad (23)$$

We have chosen the following coordinate system

$$\vec{H}_0 = \vec{h}H_0, \vec{E}_0 = \vec{h}E_0 \quad (24)$$

To determine the variable part of the magnetic field, we will use the Maxwell equations

$$\frac{\partial\vec{H}'}{\partial t} = -crot\vec{E}', \vec{H}' = \frac{c}{\omega}\left[\vec{k}\vec{E}'\right] \quad (25)$$

Considering $H' \sim e^{i(\vec{k}x-\omega t)}$ and $E' \sim e^{i(\vec{k}x-\omega t)}$ from (24), taking into account (25), we obtain the following dispersion equations for determining the frequency of current oscillations

$$\Omega^2\vec{E}' + \left(\vec{i}\,\Sigma_1 H_0 E_y' - \vec{h}\Sigma_2 H_0^2 E_z'\right)\omega - 2\Sigma_2 E_0 H_0 c\left[\vec{k}\vec{E}'\right] + \\ + \left[\Sigma_1 cE_0 E_z' - \frac{ic^2}{4\pi}\left(\vec{k}\vec{E}'\right)\right]\vec{k} = 0 \quad (26)$$

Writing down the components of the vector equation (26), we obtain the following three equations

$$\begin{cases} \Omega_1^2 E_x' + \Omega_2^2 E_y' + \Omega_3^2 E_z' = 0 \\ \Xi_1^2 E_x' + \Xi_2^2 E_y' + \Xi_3^2 E_z' = 0 \\ \Theta_1^2 E_x' + \Theta_2^2 E_y' + \Theta_3^2 E_z' = 0 \end{cases} \quad (27)$$

Here:

$$\Omega_1^2 = \Omega^2 - \frac{ic^2k_x^2}{4\pi},\ \Omega_2^2 = \Sigma_1 H_0\omega + 2\Sigma_2 E_0 H_0 k_z c - \frac{ic^2k_xk_y}{4\pi},\ \Omega_3^2 = \Sigma_1 E_0 ck_x - 2\Sigma_2 E_0 H_0 ck_y - \frac{ic^2k_xk_z}{4\pi},$$
$$\Xi_1^2 = -2\Sigma_2 E_0 H_0 ck_z - \frac{ic^2k_xk_y}{4\pi},\ \Xi_2^2 = \Omega^2 - \frac{ic^2k_y^2}{4\pi},\ \Xi_3^2 = 2\Sigma_2 E_0 H_0 ck_x + \Sigma_1 E_0 ck_y - \frac{ic^2k_yk_z}{4\pi}, \quad (28)$$
$$\Theta_1^2 = 2\Sigma_2 E_0 H_0 ck_y - \frac{ic^2k_xk_z}{4\pi},\ \Theta_2^2 = -2\Sigma_2 E_0 H_0 ck_x - \frac{ic^2k_yk_z}{4\pi},\ \Theta_3^2 = \Omega^2 - \Sigma_2 H_0^2\omega + \Sigma_1 E_0 ck_z - \frac{ic^2k_z^2}{4\pi}.$$

We obtain the following dispersion equations for determining the frequency of the current oscillation from the solution of the system of equations (28)

$$\Omega^2 = 16\pi^2\Sigma_2^2\left[\frac{\Sigma^2}{ck_z} - \frac{2ck_z}{\Sigma^2} + i2\pi^2\left(\frac{L_z}{L_x}\right)^2\right] \quad (29)$$

L_z, L_x - corresponding sample lengths.

Here

$$\Omega = \Sigma + \frac{ic^2k^2}{4\pi\omega} + \frac{i\omega}{4\pi} \quad (30)$$

When deriving the dispersion equation, we used the inequality for the electric field

$$E_0 >> uE_{char},\ u = \frac{16\pi^2\sigma_{20}^2k_y^2}{c^2k_x^2k_z^2\Delta} \quad (31)$$

$$\Sigma_2^2 = \Sigma_{20}^2\alpha^{1/2} = \Sigma_{20}^2\cdot\frac{E_x}{\Delta E_0}$$

$$E_x = \left(\frac{3D^4m_0m_a^3m_bk_0T}{\pi^2e^2\hbar^8\rho^2u_0^2}\right)^{1/2}$$

$$L_x = L_y$$

By supplying (30) to (31), we obtain the following equations for determining the frequency of the current oscillation

$$\omega^2 - 4\pi i\left[\Sigma - \frac{4\pi^2\Sigma_2 L_z}{L_x}\left(\frac{1}{2}+i\right)\right]\omega + 4\pi c^2k^2 = 0 \quad (32)$$

From solution (33), taking into account (32), we easily obtain:

$$\omega_0 = \frac{8\pi^3 \Sigma_2 L_z}{L_x}, \ \omega_1 = 2\sqrt{\pi}ck \tag{33}$$

Formulas (33) for the frequency of the current oscillation and the growth rate of the oscillation are obtained at

$$ck >> \pi\sqrt{2}\Sigma\frac{E_x}{E_0} \tag{34}$$

e.g

$$E_0 >> E_x\frac{\pi\sqrt{2}\Sigma}{ck} \tag{35}$$

Comparison of (35) with (31) is in good agreement.

DISCUSSION OF THE RESULTS

The intervals of variation of the external constant electric field are determined by applying the kinetic equation in two-valley semiconductors of the GaAs type, at which radiation of electromagnetic energy occurs. Such an unstable state occurs in a sample, the dimensions of which are $L_x = L_y$, $L_z >> L_x, L_y$, the coordinate system $\vec{H}_0 = \vec{h}H_{0z}$, $\vec{E}_0 = \vec{h}E_{0z}$, $\mu H_{0z} >> c$ and, with a different coordinate system $E_0 \perp H_0, \vec{E}_0\vec{H}_0 = E_0H_0\cos\alpha, \left[\vec{E}_0\vec{H}_0\right] = E_0H_0\sin\alpha$, a different value of theoretical research is needed. It can be seen from the CVC graph that the point $\frac{dj}{dE} = 0$ is the beginning of the oscillation, i.e. $\omega_1 = 0$ is increment. Considering $\omega = \omega_0$, $\omega_0 = 2\pi\sigma$.

$$E_0 = E_{char}\cdot\frac{c^2k^2}{\pi\Delta u_0^2} \tag{36}$$

$$u_0 = \frac{8nc^2m_a^{1/2}m_0^{1/2}}{3\sqrt{2}\Gamma(3/4)H^2}\cdot\left(\frac{m_b}{m_a}\right)^3 \tag{37}$$

With an increase in the magnetic field, the electric field increases in a square, and this can be used to regulate the instability.

[1] *J.B. Gunn.* "Microwave Oscillations of Current in III -V Semiconductors", Solid State Comm., Vol. 1, №4, p. 88, Sept. 1963.

[2] *B.I. Davydov.* "On the theory of the motion of electrons in gases and in semiconductors", ZhETF. T.7, p. 1069, 1937.

[3] *B.K. Ridley, T.B. Watkins.* "The Possibility of Negative Resistance Effects in Semiconductors", Proc.Phys.Soc. V. 7, p. 293, 1961.

[4] *E.R. Hasanov, Sh.G. Khalilova, R.K. Mustafayeva and G.M. Mammadova.* "Oscillations of Current in Two-Valley Semiconductors in a Strong Electric Field", Advanced Studies in Theoretical Physics, Vol. 15, №3, p. 145 – 152, 2021.

[5] *E.R. Hasanov, R.K. Mustafayeva, G.M. Mammadova, Sh.G. Khalilova, E.O. Mansurova,* "Excitation of Growing Waves in Impurity Semiconductors with Two Current Fluctuations in Two-Valley Semiconductors in Strong Electric and Magnetic Fields", IOSR Journal Of Applied Physics (IOSR-JAP) e-ISSN: 2278-4861.Vol. 13, p. 55-62 Jan. – Feb. 2021.

Received: 05.07.2021

CHARACTERISTICS OF AMORPHOUS Se ELECTROGRAPHIC LAYERS ON SUBSTRATES WITH OXIDE FILM

V.G. AGAYEV
Institute of Physics of ANAS
131, H.Javid ave., Baku, AZ 1143

The electrographic amorphous Se layers are prepared by Se sublimation of OSCh trade mark 17-3 on cylindrical metal substrates with barrier oxide film. The influence of film thickness on layer photoelectric characteristics is investigated. It is shown that for achieving of optimal dark and light parameters it is necessary to form the oxide film by 3μm thickness on substrate.

Keywords: photoreceptor, oxide film, barrier layer.
PACS: 07.68.+m, 72.40.+w

1. INTRODUCTION

The development of science, technique and national economics, the increase of efficiency of control by this process is accompanied by intensive information volume. In this connection the non-polygraphic methods of operating document copying and duplication on the base of industrial gage application such as diazoprocess, photography, electrography, thermography and electronography joined by general term which is the reprography. The principal difference of reprography from polygraphy is the fascimility, i.e. the supply of total identity of disposition order of image elements, their configuration, print type in original and copy.

Nowadays, the electrophotography the principles of which are connected with achievements of semiconductor physics [1] is the one of the extended and intensively developed methods of reproduction.

Electrophotography (EPh) is the set of methods and industrial gages of image obtaining on special surfaces, electric properties of which change in the correspondence with light radiation quantity accepted by these surfaces. The electrolyzed thin layer of photosemiconductor (for example, amorphous Se) marked on conducting substrate is the supersensitive one in EPh.

EPh image obtaining process is caused by physical phenomena taking place in high-ohmic semiconductor layers at their electrization, exposure and also electric interactions between charged states at revealing and transfer of the image on paper or other base. In the difference from the ordinary photography in EPh scheme of image obtaining there are additional principally new two stages which are layer electrization (sensitization) before exposure and transfer of revealed image with layer on other material.

The wide application of EPh causes the necessity in improvement of existing photoreceptors and in obtaining of new ones. The photosensitivity in visible and especially red spectrum region is the important criteria. Nowadays, the schemes of xerographic image reproduction based on use of amorphous Se, compounds by A^2B^6 type, organic semiconductors and etc. are realized. The fabrication technique of EPh layers of photosemiconductors of $A^2B^3{}_2$ $C^6{}_4$ type having the high photosensitivity in visible spectrum region is developed. The investigation on photoreceptor creation on the base of amorphous silicon enriched by hydrogen [12] are carried out.

2. EXPERIMENT AND RESULT DISCUSSION

Se which is elementary semiconductor attracts the attention of the investigators by their unique properties. It has the high photosensitivity, it can be obtained in amorphous and crystalline (trigonal and monoclinic) states. All this makes it unchangeable at creation of different transformers (first power rectifiers, photoreceptors, vidicons, photo-isolator and etc.). Se high technology (low melting point, the possibility of any form marking on the surface and etc.) is important. Wide-ranging use of Se in different technique region constantly stimulate the investigation of its properties all over the world.

The photoreceptors on the base of amorphous Se have the high EPh parameters (they are well chargeable ones and have photosensitivity), but at the same time they have disadvantages. They are weakly sensitive to red light, the layers of amorphous Se crystallize under influence of many factors and break down in the result of explosure [3].

Trigonal Se is known as photosemiconductor with spectral sensitivity in spectrum visible region. Usually, the layers from trigonal Se are prepared by dispersion of its particles in polymer bonder layer and marking of suspension on conducting substrate. They have well photosensitivity, but simultaneously have relatively low initial potential of charging and dark semi-drop that is the result of Se high conductivity [4].

The elimination of above-mentioned disadvantages belonging to layers from amorphous Se prepared in complex vacuum equipment and search of the improving ways of their parameters and characteristics is the task of the given work. The search of relevant ways is carried out with this aim.

Se electrographic layer (SEL) is the complex system which consists of the conducting substrate, barrier (shutoff) layer, multifunctional layer of photosemiconductor and often the external protective layer. The physical properties of such systems are studied all over the World, however, the many

131, H.Javid ave, AZ-1143, Baku
ANAS, Institute of Physics
E-mail: jophphysics@gmail.com

questions stay unsolved ones up to now, in particular, the interconnection between system composite elements in formation of photoreceptor property complex isn't established. So, by others opinion the oxide film on substrate carries out the several functions: it carries out the interface in boundary substrate – photosemiconductor, improves the photosemiconductor adhesion to substrate, makes barriers preventing the carrier injection from substrate into photosemiconductor and reactive diffusion between them. Thus, the oxide film should significantly influence on photoreceptor parameters. Concerning this, oxide film thickness and the time of substrate chemical oxidation time which changes in interval (0,1–15min) are chosen in the capacity of alternative parameters.

The oxide films on metallic (duralumin) substrate can be obtained by thermal oxidation in oxygen atmosphere, ion-plasma spraying, spraying of aluminum in oxygen atmosphere, pyrolysis of hetero-organic compounds, anode oxidation in electrolytes and by chemical oxidation [5].

Se electrographic layers the oxide films of which on duralumin substrates are formed by chemical oxidation in solution containing the chrome anhydride (3-7g/l), sodium fluoride (3-4g/l) and orthophosphoric acid (40-50g/l), are investigated. The oxidation is carried out at 25°C and curing time in solution is (0,1-15) min. This supplies the formation of oxide films with thickness from 40 Å up to 5μm.

The film thickness is defined by capacity method with the help of bridge L2-7 at frequency 465kHz (dielectric constant of oxide film is equal to 8). The measurements show that film thickness d monotonously increases with tendency to saturation at $t_{xo} \geq 12$ min with increase of oxidation duration t_{xo}. The solution aging time plays the significant role. The most thickness (d=5μm) forms at the use of fresh solution whereas the films of less thickness form in used solutions though the grow character d on t_{xo} is the same. The quality of oxide film begins to worsen with t_{xo} increase.

After oxidation the cylindrical substrates are degassed at 140°C during 60 min and Se by trend mark OSCh 17-3 is marked by sublimation method during 25 min at program change of temperature substrate from 40 up to 82±0,5°C. The thickness of Se layer is 60-85μm. The samples have the form of ring fragments by height 100mm. Their EPh parameters are investigated on test bed prepared on the base of apparatus EP-300K2 (dynamic mode). The parameters are measured after 30 minutes of the charge-exposure cycle. The dark drop time of the potential $\tau_{1/2}$ and the velocity of its dark relaxation υ_{15} (15sec after charging), integral photosensitivity S_{int} and spectral distribution of photosensitivity S_λ in the interval of wave length 300 – 1000nm are defined. The light source is graduated by radiation compensated thermo-element PTH-30.

The nature of interface photosemiconductor-substrate is the determinative factor of potential dark drop. It is important that contact substrate-semiconductor should be shutoff for the carriers even if for one sign. The contact region substrate-semiconductor should be barrier for the electrons preventing their injection from the substrate to the layer at relatively high electric field strength at positive photoreceptor electrization for surface charge retention. The measurements show (Fig.1) that $\tau_{1/2}$ increases with increase of oxide film thickness d passing through at $d \simeq 2{,}5$τm ($t_{xo} \simeq 5$min.) and it strongly decreases with further thickness increase. The change υ_{15} also has the extreme character with minimum at $d \simeq 2{,}5$μm (Fig.1). The coincidence of d dependences on t_{xo}, $\tau_{1/2}$ and υ_{15} on d allow us to suppose that the extremal change $\tau_{1/2}$ and υ_{15} is caused by the following reasons. The oxide film forms on the substrate at interaction with solution and its growth slows after achieving of the thickness $d \simeq 3$μm.

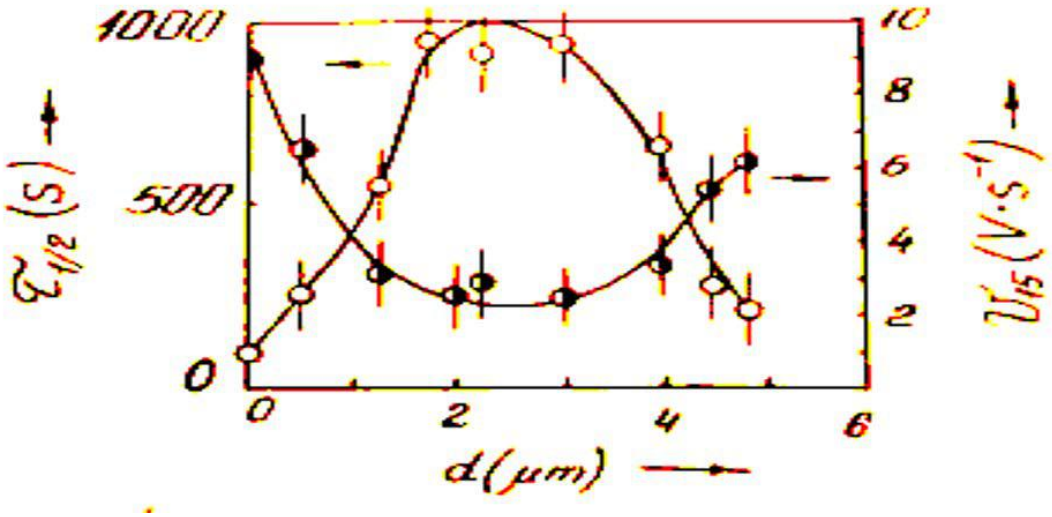

Fig.1. The dependence of dark drop time $\tau_{1/2}$ and relaxation rate of surface potential υ_{15} on d.

The barrier layer efficiency increases with d increase and this leads to increase of $\tau_{1/2}$ and decrease of υ_{15}. The further storage in the solution (t_{xo}>5min.) leads to undercutting of oxide film as a result of which the obtained films are porous ones with defect structure and dirty ones. As a result, the oxide film conditions worsen

and the efficiency of anti-injection barrier ($\tau_{1/2}$ decreases, υ_{15} increases) increases.

EL photosensitivity is defined by the quantity of incident quantums on layer unit of area per definite time, i.e. by exposition $H=L\tau_0$ (L is illumination, τ_0 is time of exposure). Note that near 20% light energy with λ=200-2500nm reflects from SEL [6]. The generally accepted technique of photosensitivity definition doesn't exist. Sometimes it is estimated by contrast of electric latent image, residual potential, semi-drop time of initial potential at the given exposure. Last time the photosensitivity in foreign literature is defined by the value of exposure supplying the drop of initial potential from 1000 up to 50V. S_{int} of investigated SEL defined by potential semi-drop in the dependence on d oxide film thickness, is shown in Fig.2.

The curve has the extremal character. S_{int}=0,66(Lx·sec)$^{-1}$ and it is observed at $d\simeq$ 3 μm. The further increase leads to strong decrease S_{int} up to 0,42 (Lx·sec)$^{-1}$.

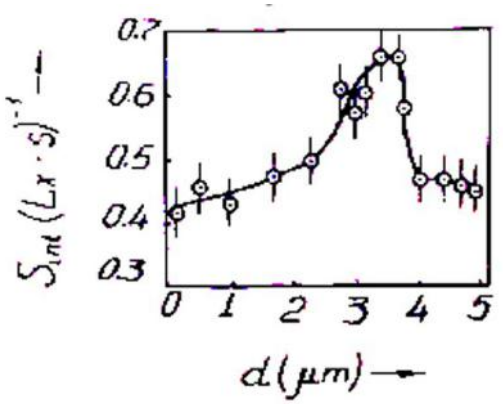

Fig.2. The dependence of S_{int} on d.

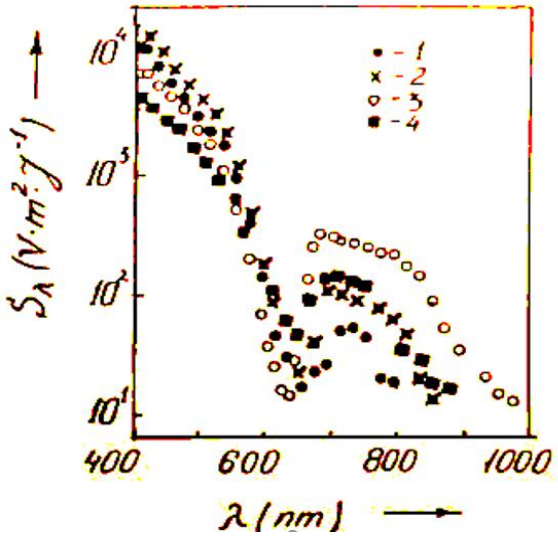

Fig.3. The spectral distribution of SEL photosensitivity at different thicknesses of oxide films.

The necessity of definition of S_{int} and S_λ of SEL under conditions corresponding to their work in the different systems appears very often. As exposure time in such conditions is given by system kinematics then for S_λ definition by semi-drop criterion it is necessary to give the illumination L_λ supplying this criterion at different λ. However, these conditions aren't correspond to exploitation ones that's why it is necessary to define the spectral distribution of photosensitivity SEL as $S_\lambda=\Delta u/L_\lambda\cdot\tau_0$ (Δu is contrast in V, L_λ in Vt/m^2, $\tau_0\simeq$1c for apparatus EP_300K2 at the given sizes of monochromator slot).

S_λ measurements of SEL with different oxide film thickness on substrate reveal the presence of two maximums: in blue (λ=410nm) and red (λ=710nm) spectrum regions (Fig.3).

The photosensitivity in blue region weakly changes with d increase whereas the photosensitivity in the red region changes significantly (≥5 times).

The exiton-like (bound) electron-hole couples in surficial photoreceptor region (in depth $\leq 1\mu m$) are generated at SEL exposure by strongly absorbed light ($\lambda\leq$410nm). The photosensitivity is defined by monopolar carrier drift and photoreceptor surficial region plays the dominating role, the nature of border region of photosemiconductor-substrate region isn't significant.

The electrons and holes excite from impurity layers in the thickness of amorphous selenium at illumination of SEL by weakly absorbed light (λ>650nm). The electrons drifting to layer surface (it is possible the electron attachment) neutralize the positive surface charge. The ionized donor centers and captured electrons create the volume charge leading the layer thickness efficiency corresponding to increase of capacity and finally to decrease of surface potential. The holes excited in amorphous selenium by weakly absorbed light drift to substrate and neutralize the negative compensating charge that also leads to decrease of surface potential in accompany of appearing volume charges taking under consideration the above-mentioned phenomena. Besides, the light with λ>650nm achieved the trigonal layer, excites the electron-hole couples. The holes drifting in the sublayer thickness (it is possible their attachment) neutralize the compensating charge. The electrons drifting in the amorphous selenium neutralize the surface charge. Also, it is possible the formation of volume charges, capacity change and etc. These phenomena cause SEL photosensitivity in red region. In order to avoid the volume charge accumulation in photoreceptor leading to fatigue effects it is charged in negative crown and lighted by white light before beginning of the following cycle charge-exposure. As SEL is complex multilayer system then for the explanation of extreme change of photosensitivity in red region on d it is necessary to take under consideration whole phenomenon diversity taking place in layer thickness and in border region to substrate.

The dependence of curve maximum of photosensitivity spectral distribution S_m of SEL in red region on oxide film thickness d is constructed. S_m achieves maximum value at $d\simeq$ 3μm. Such dependence of S_m on d can be caused by the following facts. The dense and qualitative oxide film which causes to formation of trigonal selenium sublayer homogeneous by phase and uniform on thickness, forms and this layer

defines S_m in the beginning oxidation process up to $d \simeq 3\mu m$. Simultaneously, the dense oxide film effectively prevents to carriers. The defects, labyrinths form in oxide film with further d increase. It enriches by impurities and it can inject carriers into layer. The sublayer of Se trigonal layer forming on such thin film also be heterogeneous, defect and dirty by different impurities. All this can lead to the decrease of photosensitivity, worsen the layer dark characteristics.

The transient relaxation phenomena leading to the stabilization of structures and parameters take place after 20 hours after evaporation of SEL. After long-term storage of SEL (6 months and more) in ordinary conditions and darkness the significant change of S_{int} and S_m aren't observed. It evidences about the fact that the existing changes of structures and properties in investigated SEL don't take place.

Thus, it is necessary to form the oxide film of $3\mu m$ thickness on substrate for achieving of optimal dark and light parameters of SEL.

---

[1] *R. Maffert.* Electrography. M., "World", 1968.
[2] *G.B. Abdullayev, V.G. Agayev.* Invention certificate. USSR:
[3] 467315 (1974), 560200(1977), 627707(1978), 704395(1979), 1170413(1985), 1176299(1985), 1301169(1986), 1403010(1988), 1466504(1988), 1568016(1990), 1675837(1991), 1730608(1992), 1807442(1992).
[4] *N.I. Ibragimov, V.G. Agayev.* Thin Solid Films. v.196, pL1-L3, 1991.
[5] *N.I. Ibragimov,V.G.Agayev, Z.M. Abutalibova.* Thin Solid Films, v.359, p.125-126, 2000.
[6] *V.D. Korzo, V.A. Kurochkin, V.P. Demin.* Films from hetero-organic compounds in radioelectronics. M., Energy, 1973.
[7] *I.B. Shneydman.* Electrography on Se layers. M., engineering. 1982.

Received: 12.07.2021

THE CONFINED HARMONIC OSCILLATOR AS AN EXPLICIT SOLUTION OF THE POSITION-DEPENDENT EFFECTIVE MASS SCHRODINGER EQUATION WITH MORROW-BROWNSTEIN HAMILTONIAN

E.I. JAFAROV, A.M. JAFAROVA, S.M. NAGIYEV, S.K. NOVRUZOVA
Institute of Physics, Azerbaijan National Academy of Sciences
Javid ave. 131, AZ1143, Baku, Azerbaijan

Exactly-solvable confined model of the non-relativistic quantum harmonic oscillator with Morrow-Brownstein kinetic energy operator $H_0 = M^{\alpha}(x)\hat{p}_x M^{\beta}(x)\hat{p}_x M^{\alpha}(x)/2$ (with $2\alpha + \beta = -1$) is proposed. Corresponding position-dependent effective mass Schrödinger equation in the canonical approach is solved in position representation. Explicit expressions of both wavefunctions of the stationary states and discrete energy spectrum have been found. It is shown that the energy spectrum has non-equidistant form and depends on both confinement parameter a and Morrow-Brownstein parameter α. Wavefunctions of the stationary states in position representation are expressed in terms of the Gegenbauer polynomials. At limit $a \to \infty$, both energy spectrum and wavefunctions recover well-known equidistant energy spectrum and wavefunctions of the stationary non-relativistic harmonic oscillator expressed by Hermite polynomials. Position dependence of the effective mass also disappears under the same limit.

Keywordas: Morrow-Brownstein kinetic energy operator, confined harmonic oscillator model, exact solution, Gegenbauer polynomials, non-equidistant energy spectrum, position-dependent effective mass
PACS: 03.65.-w; 02.30.Hq; 03.65.Ge

1. INTRODUCTION

One-dimensional harmonic oscillator is one of the attracting problems of the quantum theory that has enormous applications in the different scientific branches of the modern physics and technologies [1]. Exact solubility of this problem within different approaches can be considered as its main attractive property. Explicit solution of its stationary Schrödinger equation within the canonical approach in the position or momentum representation is best known case with wide applications in physics and mathematics. Here, obtaining explicit expressions of the wavefunctions of the stationary states and discrete energy spectrum formally means exact solution of the problem under study. Stationary Schrödinger equation within the canonical approach in the position representation leads to the second order differential equation, whose eigenfunctions vanishing at infinity are wavefunctions of the one-dimensional quantum harmonic oscillator expressed in terms of the Hermite polynomials and eigenvalues are discrete energy spectrum with equidistant energy levels spacing [2]. This is not only the explicit quantum mechanical realization of the one-dimensional harmonic oscillator problem with wavefunctions vanishing at infinity. Explicit solved model of the one-dimensional non-relativistic harmonic oscillator is realized within non-canonical approach, whose wavefunctions of the stationary states are expressed through the generalized Laguerre polynomials [3]. Explicit realizations of the quantum harmonic oscillator with wavefunctions vanishing at infinity within the different relativistic formalisms also exist [4-6]. Another approach for exact solution of the quantum harmonic oscillator problem with wavefunctions vanishing at infinity is study of the problem in the discrete position of momentum space. Usually, wavefunctions of such models are expressed in terms of the finite- or infinite-discrete orthogonal polynomials [7-14]. One need to note another interesting hybrid model that is realized as quantum harmonic oscillator with wavefunctions vanishing at infinity and its wavefunctions are expressed by Meixner and generalized Laguerre polynomials depending on the discreteness or continuous nature of the configuration representation [15]. However, quantum-mechanical explicit solution of the harmonic oscillator problem in the infinite-continuous configuration space is still open. It is obvious that the wavefunctions of the stationary states of the explicitly solved quantum harmonic oscillator should differ from above listed models with property of vanish at finite region. Some attempts have been done to solve this oscillator problem, but all these attempts lead to approximate expressions both wavefunctions and energy spectrum [16-23]. Taking into account the role that such a harmonic oscillator model can play in the development of different branches of physics, especially, nanotechnologies and low dimensional physics, we suppose explicit quantum mechanical solution of the harmonic oscillator confined in finite region within the framework of the position-dependent effective mass formalism. Significance of the position-dependent effective mass formalism mainly is its appearance in quantum-mechanical solutions due to experimental data coming from solid state physics and necessity of its correct interpretation within quantum theory laws. For the first time, [24] used position-dependent band structure formalism in order to explain seminal experiment on the tunneling into superconductors [25, 26]. Then, this formalism was developed into the assumption that position-dependent band structure formalism should be simulated by position-dependent effective mass $M(x)$Based on this assumption, the non-relativistic Hermitian kinetic energy operator with effective mass varying with position was introduced in [27]. It is now known as BenDaniel-Duke kinetic energy operator:

$$\widehat{H}_O^{BD} = \frac{1}{2}\hat{p}_x \frac{1}{M(x)}\hat{p}_x \qquad (1)$$

131, H.Javid ave, AZ-1143, Baku
ANAS, Institute of Physics
E-mail: jophphysics@gmail.com

Later, one-dimensional model of an abrupt heterojunction with the same lattice constant throughout the structure was considered theoretically with assumption that all primitive lattice cells on two opposite sides of the hetero-interface differ from each other and another kind of non-relativistic kinetic energy operator with position-dependent effective mass was introduced as a result of the study of the problem of the connection rules for effective-mass wave functions across an abrupt heterojunction between two different semiconductors [28]. It is known as Zhu-Kroemer kinetic energy operator:

$$\hat{H}_O^{ZK} = -\frac{1}{\sqrt{M(x)}}\hat{p}_x^2\frac{1}{M(x)} \tag{2}$$

Further, Zhu-Kroemer kinetic energy operator formalism was supported as a model of an abrupt heterojunction between two different semiconductors via more general investigation in [29, 30]. It resulted introduction of the more generalized non-relativistic Hermitian operator with position-dependent effective mass that is known at present as Morrow-Brownstein kinetic energy operator:

$$\hat{H}_O^{MB} = \frac{1}{2}M^{\alpha}(x)\hat{p}_x M^{\beta}(x)\hat{p}_x M^{\alpha}(x), \;\; 2\alpha+\beta=-1 \tag{3}$$

It is obvious that BenDaniel-Duke and Zhu-Kroemer kinetic energy operators with $\alpha = 0$ ($\beta = -1$) and $\alpha = -\frac{1}{2}$ ($\beta = 0$)are special cases of Morrow-Brownstein kinetic energy operator. Schrödinger equation with position-dependent effective mass involving all three listed above kinetic energy operators is studied thoroughly in a lot of published works. For example, exact solutions of the BenDaniel-Duke Schrödinger equation with different potentials are obtained for position-dependent effective mass of exponential behavior by using coordinate transformation method in [31]. Also, [32] generalized harmonic oscillator model through explicit solution of the corresponding Morrow-Brownstein Schrödinger equation with position-dependent effective mass and obtains explicit expressions of the wavefunctions of the stationary states and energy spectrum. A one-dimensional harmonic oscillator with position-dependent effective mass is studied in [33] and corresponding BenDaniel-Duke Schrödinger equation is solved explicitly in terms of modified Hermite polynomials. Position-dependent effective mass formalism is not only powerful tool in the solution of the Schrödinger equation. For example, the Duffin–Kemmer–Petiau equation with position-dependent mass for relativistic spin-1 particles under Coulomb interaction as well as in the presence of Kratzer-type potential is also studied analytically leading to obtaining asymptotical solutions in terms of the eigenvalues and eigenvectors [34, 35].

Present paper is structured as follows: in Section 2, the basic known information about the one-dimensional quantum harmonic oscillator is presented. This information covers explicit expressions of the wavefunctions of the stationary states and energy spectrum obtained via solution of the non-relativistic Schrödinger equation within canonical approach. Section 3 is devoted to the solution of the Morrow-Brownstein Schrödinger equation with position-dependent effective mass for the confined quantum harmonic oscillator model. Explicit expressions of the both wavefunctions of the stationary states in terms of the Gegenbauer polynomials and non-equidistant energy spectrum are presented in this section as well as it is shown that obtained wavefunctions possess correct orthogonality relations. Brief discussion of the obtained results is given in Section 4. It is shown that both wavefunctions and energy spectrum correctly recover their unconfined expressions under certain limit.

2. NON-RELATIVISTIC QUANTUM HARMONIC OSCILLATOR UNDER THE CANONICAL APPROACH: WAVEFUNCTIONS IN TERMS OF HERMITE POLYNOMIALS AND EQUIDISTANT ENERGY SPECTRUM

Solution of the non-relativistic quantum harmonic oscillator is well known and it is obtained from the following stationary Schrödinger equation in position representation

$$\left[\frac{\hat{p}_x^2}{2m} + V(x)\right]\psi(x) = E\psi(x) \tag{4}$$

In order to solve this equation, first of all it is necessary to define non-relativistic harmonic oscillator potential that has the following form:

$$V(x) = \frac{m\omega^2 x^2}{2} \tag{5}$$

Here m and ω are position-independent mass and angular frequency of the non-relativistic quantum harmonic oscillator. Then, it is necessary to define if this equation is going to be solved under canonical or non-canonical approach. Taking into account that we are interested in the solution under the canonical approach, then definition of the one-dimensional momentum operator under this approach is as follows

$$\hat{p}_x = -i\hbar\frac{d}{dx}, \tag{6}$$

whose substitution to Schrödinger equation (4) means that it is written in the canonical approach. Finally, one needs to look for explicit non-relativistic harmonic oscillator solutions with vanishing wavefunctions at infinity. Then, taking into account this statement and both definitions (5) and (6) in eq. (4) one easily obtains the following well-known second order differential equation:

$$\frac{d^2\psi}{d^2x} + \frac{2m}{\hbar^2}\left(E - \frac{m\omega^2x^2}{2}\right)\psi = 0 \tag{7}$$

Explicit solutions allow to obtain eigenfunctions of this equation, which are wavefunctions of the stationary states in the position representation

$$\psi \equiv \psi_n(x) = \frac{1}{\sqrt{2^n n!}}\left(\frac{m\omega}{\pi\hbar}\right)^{\frac{1}{4}} e^{\frac{m\omega x^2}{2\hbar}} H_n\left(\sqrt{\frac{m\omega}{\hbar}}x\right), \tag{8}$$

and eigenvalues of this equation in terms of discrete equidistant energy spectrum

$$E \equiv E = \hbar\omega\left(n+\frac{1}{2}\right),\ n = 0,1,2,\ldots, \tag{9}$$

where, $H_n(x)$ are Hermite polynomials defined through ${}_2F_0$ hypergeometric functions as follows [36]:

$$H_n(x) = (2x)^n\ {}_2F_0\left(-\frac{n}{2}\cdot -\frac{(n-1)}{2}; -\frac{1}{x^2}\right) \tag{10}$$

Hermite polynomials satisfy the following orthogonality relation:

$$\frac{1}{\sqrt{\pi}}\int_{-\infty}^{\infty} e^{-x^2} H_m(x)H_n(x)dx = 2^n n!\,\delta_{mn}, \tag{11}$$

therefore, normalized wavefunctions (8) based on (11) also satisfy similar orthogonality relation:

$$\int_{-\infty}^{\infty} \psi_m^*(x)\,\psi_n(x)dx = \delta_{mn} \tag{12}$$

In next section, we are going to generalize these expressions to confined Morrow-Brownstein quantum oscillator case.

3. CONFINED MORROW-BROWNSTEIN QUANTUM HARMONIC OSCILLATOR: WAVEFUNCTIONS IN TERMS OF GEGENBAUER POLYNOMIALS AND NON-EQUIDISTANT ENERGY SPECTRUM

We start from the stationary Schrödinger equation with position-dependent effective mass $M(x)$ and introduce confined harmonic oscillator potential as follows:

$$V(x) = \begin{cases} \frac{M(x)\omega^2x^2}{2}, & -a < x < a, \\ \infty, & x = \pm a. \end{cases} \tag{13}$$

Taking into account Morrow-Brownstein kinetic energy operator (13), it is clear that we need to solve the stationary Schrödinger equation with the following Hamiltonian:

$$H^{MB} = \frac{1}{2}M^{\alpha}(x)\hat{p}_x M^{\beta}(x)\hat{p}_x M^{\alpha}(x) + \frac{m\omega^2x^2}{2} \tag{14}$$

We are going to solve the stationary Schrödinger equation within canonical approach, therefore, substitution of the momentum operator $\hat{p}_x$ (6) to (14) and simple straightforward computations lead to the following expression of Hamiltonian H^{MB}:

$$H^{MB} = -\frac{\hbar^2}{2M}\left[\frac{d^2}{dx^2} - \frac{M'}{M}\frac{d}{dx} + \alpha\frac{M''}{M} - \alpha(\alpha+2)\left(\frac{M'}{M}\right)^2\right] + \frac{M\omega^2x^2}{2}, \tag{15}$$

with $M \equiv M(x)$.

It is clear that defining explicitly position-dependent effective mass $M \equiv M(x)$, one can try to solve explicitly the Schrödinger equation with Hamiltonian (15). We require that position-dependent effective mass $M(x)$ has to satisfy the following conditions:

- $M(x)$ should recover correct constant mass m at origin of position $x = 0$ and then under the limit $a \to \infty$;
- Confinement effect at values of position $x = \pm a$ should be achieved via analytical definition of the position-dependent effective mass $M(x)$;
- Stationary Schrödinger equation for the Hamiltonian H^{MB} (15) should be explicitly solvable and then its solutions should recover non-relativistic Hermite oscillator solutions under the limit $a \to \infty$;.

Based on listed above conditions, we define the following analytical expression for the position-dependent effective mass $M(x)$:

$$M \equiv M(x) = \frac{a^2 m}{a^2 - x^2} \tag{16}$$

It is clear that first condition is satisfied easily, because, $M(0) = m$ as well as

$$\lim_{a\to\infty} \frac{a^2 m}{a^2 - x^2} = m \tag{17}$$

Concerning second condition, one observes that harmonic oscillator potential (13) with position-dependent effective mass $M(x)$ (16) possesses the correct infinite high walls boundary conditions

$$V(-a) = V(a) = \infty \tag{18}$$

Then, we need only to prove the satisfaction of the third condition. Therefore, we have to solve explicitly stationary Schrödinger equation for the Hamiltonian H^{MB} (15). Simple computations show that

$$\frac{M'}{M} = \frac{2x}{a^2 - x^2},$$
$$\frac{M''}{M} = \frac{2x}{a^2 - x^2} + \frac{8x^2}{(a^2 - x^2)^2}$$

Taking them into account in Hamiltonian H^{MB} (15) we have

$$H^{MB} = -\frac{\hbar^2}{2M}\left[\frac{d^2}{dx^2} - \frac{2x}{a^2-x^2}\frac{d}{dx} + \frac{2\alpha}{a^2-x^2} - \frac{4\alpha^2 x^2}{(a^2-x^2)^2}\right] + \frac{M\omega^2 x^2}{2}, \tag{19}$$

Corresponding Schrödinger equation becomes the following second order differential equation:

$$\left[\frac{d^2}{dx^2} - \frac{2x}{a^2-x^2}\frac{d}{dx} + \frac{2\alpha}{a^2-x^2} - \frac{4\alpha^2 x^2}{(a^2-x^2)^2}\right]\psi + \left(\frac{c_0}{a^2-x^2} - \frac{c_2}{(a^2-x^2)^2}\right)\psi = 0, \tag{20}$$

with $c_0 = \frac{2ma^2E}{\hbar^2}$ and $c_2 = \frac{m^2\omega^2a^4}{\hbar^2}$.

Now, introduction of the dimensionless variable $\xi = \frac{x}{a}$ with $\frac{d}{dx} = \frac{1}{a}\frac{d}{d\xi}$ and $\frac{d^2}{dx^2} = \frac{1}{a^2}\frac{d^2}{d\xi^2}$ leads to the following second order differential equation:

$$\psi'' + \frac{\tilde{\tau}}{\sigma}\psi' + \frac{\tilde{\sigma}}{\sigma^2}\psi = 0 \tag{21}$$

Here

$$\tilde{\tau} = -2\xi, \tag{22}$$

$$\sigma = 1 - \xi^2, \tag{23}$$

and

$$\tilde{\sigma} = (2\alpha + c_0) - (4\alpha^2 + 2\alpha + c_0 + c_2)\xi^2 \tag{24}$$

We apply Nikiforov-Uvarov method for solution of eq.(21). This method is applicable to differential equations with σ and $\tilde{\sigma}$ being polynomials at most of second degree and $\tilde{\tau}$ being a polynomial at most of first degree [37]. We look for solution of eq.(21) as follows:

$$\psi = \varphi(\xi)y \tag{25}$$

Here, $\varphi(\xi)$ is defined by the following manner:

$$\varphi(\xi) = e^{\int \frac{\pi(\xi)}{\sigma(\xi)} d\xi}, \tag{26}$$

with $\pi(\xi)$ also being a polynomial at most of first degree.

Simple computations with substitution of (25) in eq.(21) lead to the following differential equation for y:

$$y'' + \frac{\tilde{\tau}}{\sigma}y' + \frac{\tilde{\sigma}}{\sigma^2}y = 0 \tag{27}$$

Here

$$\tau = 2\pi + \tilde{\tau}, \tag{28}$$

And

$$\tilde{\sigma} = \tilde{\sigma} + \pi^2 + \pi(\tilde{\sigma} - \sigma') + \pi'\sigma \tag{29}$$

Already, the function $\pi(\xi)$ has been defined as a polynomial at most of first degree. We are going to choose the coefficients of $\pi(\xi)$ in $\tilde{\sigma}$ (29) will be divisible by σ as follows:

$$\tilde{\sigma} = \lambda\sigma \tag{30}$$

Then, we have to obtain explicit expression of $\pi(\xi)$ by solving the following quadratic equation:

$$\pi^2 + \pi(\tilde{\sigma} - \sigma') + \tilde{\sigma} - \mu\sigma = 0, \tag{31}$$

with definition $\mu = \lambda - \pi'$. Taking into account that $\tilde{\tau} - \sigma' = 0$, quadratic equation (31) will be simplified as follows:

$$\pi^2 + \tilde{\sigma} - \mu\sigma = 0 \tag{32}$$

Its solution in general can be written as

$$\pi = \varepsilon\sqrt{(\mu - 2\alpha - c_0) + (4\alpha^2 + 2\alpha + c_0 + c_2 - \mu)\xi^2}, \varepsilon = \pm 1$$

Two cases (four solutions) satisfy the condition for $\pi(\xi)$ being a polynomial at most of first degree:

$$\pi(\xi) = \begin{cases} \varepsilon q\xi, & \mu = 2\alpha + c_0 \\ \varepsilon q, & \mu = 4\alpha^2 + 2\alpha + c_0 + c_2 \end{cases} \quad (33)$$

where, $q = \sqrt{(4\alpha^2 + c_2)}$. Finding explicit expressions of functions $\pi(\xi)$ and $\sigma(\xi)$ now one can also obtain explicit expression of $\varphi(\xi)$ from (26). Through simple computations we obtain that $\varphi(\xi) = (1 - \xi^2)^{-\frac{1}{2}\varepsilon q}$ for case $\mu = 2\alpha + c_0$ and $\varphi(\xi) = (\frac{1+\xi}{1-\xi})^{\frac{1}{2}\varepsilon q}$ for case $\mu = 4\alpha^2 + 2\alpha + c_0 + c_2$.

Finiteness property of the wavefunction at points $\xi + \pm 1$ (or $x = \pm a$) (i.e., $\lim_{\xi \to \pm 1} \varphi(\xi) = 0$ should be satisfied at all) requires that the case $\mu = 2\alpha + c_0$ should be chosen and the condition $\varepsilon = -1$ should be satisfied for $\varphi(\xi)$. These consequences lead to the following final expressions of $\pi(\xi)$ and $\varphi(\xi)$:

$$\pi = -q\xi = -\sqrt{4\alpha^2 + c_2}\,\xi,$$

$$\varphi(\xi) = (1 - \xi^2)^{\frac{q}{2}}$$

Now, one can easily compute multiplier λ introduced in (30):

$$\lambda = 2\alpha + c_0 - q.$$

Eq.(27) via substitution of (30) will have the following simpler form:

$$\sigma y'' + \tau y' + \lambda y = 0.$$

Taking into account that τ also can be easily computed from (28) and it is equal to

$$\tau = -2(q + 1)\xi,$$

then, we need to look for the polynomial solution of the equation

$$(1 - \xi^2)y'' - 2(q + 1)\xi y' + (2\alpha + c_0 - q)y = 0 \quad (34)$$

Comparing eq.(34) with the following second order differential equation for the Gegenbauer polynomials [36]

$$(1 - x^2)\overline{y''} - \left(2\bar{\lambda} + 1\right)x\overline{y'} + n\left(n + 2\bar{\lambda}\right)\bar{y} = 0, \bar{y} = C_n^{\bar{\lambda}}(x),$$

we obtain the following non-equidistant energy spectrum

$$E \equiv E_n^{MB} = \hbar\sqrt{\omega^2 + \frac{4\alpha^2\hbar^2}{m^2a^4}}\left(n + \frac{1}{2}\right) + \frac{\hbar^2}{2ma^2}(n^2 + n - 2\alpha), \quad (35)$$

and wavefunctions of the stationary states

$$\psi \equiv \psi_n^{MB}(x) = C_n^{MB}\left(1 - \frac{x^2}{a^2}\right)^{\frac{1}{2}\sqrt{\frac{m^2\omega^2a^4}{\hbar^2} + 4\alpha^2}} C_n^{\sqrt{\frac{m^2\omega^2a^4}{\hbar^2} + 4\alpha^2} + \frac{1}{2}}\left(\frac{x}{a}\right), \quad (36)$$

Where $C_n^{\bar{\lambda}}(x)$ are Gegenbauer polynomials defined in terms of the ${}_2F_1$ hypergeometric functions as follows:

$$C_n^{\bar{\lambda}}(x) = \frac{(2\bar{\lambda})_n}{n!}\,{}_2F_1\left(\begin{matrix} -n, n + 2\bar{\lambda} \\ \bar{\lambda} + 1/2 \end{matrix}; \frac{1 - x}{2}\right), \bar{\lambda} \neq 0 \quad (37)$$

and the normalization factor C_n^{MB} being equal to

$$C_n^{MB} = 2^{\sqrt{\frac{m^2\omega^2a^4}{\hbar^2} + 4\alpha^2}}\Gamma\left(\sqrt{\frac{m^2\omega^2a^4}{\hbar^2} + 4\alpha^2} + \frac{1}{2}\right)\sqrt{\frac{\left(n + \sqrt{\frac{m^2\omega^2a^4}{\hbar^2} + 4\alpha^2} + \frac{1}{2}\right)n!}{\pi a\Gamma\left(n + 2\sqrt{\frac{m^2\omega^2a^4}{\hbar^2} + 4\alpha^2} + 1\right)}} \quad (38)$$

is defined from the orthogonality relation for Gegenbauer polynomials $C_n^{\bar{\lambda}}(x)$ of the following form

$$\int_{-1}^{1}(1-x^2)^{\bar{\lambda}-\frac{1}{2}}C_m^{\bar{\lambda}}(x)C_n^{\bar{\lambda}}(x)dx=\frac{\pi\Gamma(n+2\bar{\lambda})2^{1-2\bar{\lambda}}}{\{\Gamma(\bar{\lambda})\}^2(n+\bar{\lambda})n!}\delta_{nm},$$

that is valid within preliminary conditions $\bar{\lambda}>-\frac{1}{2}$ and $\bar{\lambda}=0$. Therefore, wavefunctions of the stationary states in the position representation (36) are also orthogonal in the finite range $-a<x<a$:

$$\int_{-a}^{a}[\psi_m^{MB}(x)]^*\,\psi_n^{MB}(x)=\delta_{nm} \qquad (40)$$

As well as explicit expressions of the energy spectrum (35) and the wavefunctions (36) are obtained, this proves exactly solubility of the quantum system under consideration within that we already defined position-dependent effective mass $M(x)$. We will discuss their behaviour as well as correct limit conditions under the limit $a\to\infty$ below.

4. DISCUSSIONS AND CONCLUSIONS

Taking into account that both energy spectrum and wavefunctions of the stationary states of the confined oscillator problem under study are known explicitly, one can discuss their different properties and special case behaviour. First of all, First of all, obtained energy spectrum (35) is not equidistant. This property is its main difference from the energy spectrum of the Hermite oscillator. We note in introduction that Morrow-Brownstein kinetic energy operator depends from the parameter α that is bounded with another parameter β via the restriction $2\alpha+\beta=-1$. This is only the restriction for α parameter, therefore, its appearance under square root in first term of the expression of the energy spectrum (35) drastically changes its behaviour. We briefly note that for imaginary values of α square root $\sqrt{\omega^2+\frac{4\alpha^2\hbar^2}{m^2a^4}}$ can be also imaginary and this case with complex energy spectrum would have further attractive applications. Another important property of the non-equidistant energy spectrum of the Morrow-Brownstein model is that there is restriction on its positivity that mathematically can be written as

$$2qe_n>e_n^2-2\alpha-\frac{1}{4},$$

with $e_n=E_n/\hbar\omega$.

Already (17) proves correct limit of position-dependent mass to homogeneous one at $a\to\infty$. Similar limit relation exists for energy spectrum (35) that is the following:

$$\lim_{a\to\infty}E_n^{MB}=\hbar\omega\left(n+\frac{1}{2}\right)=E_n \qquad (41)$$

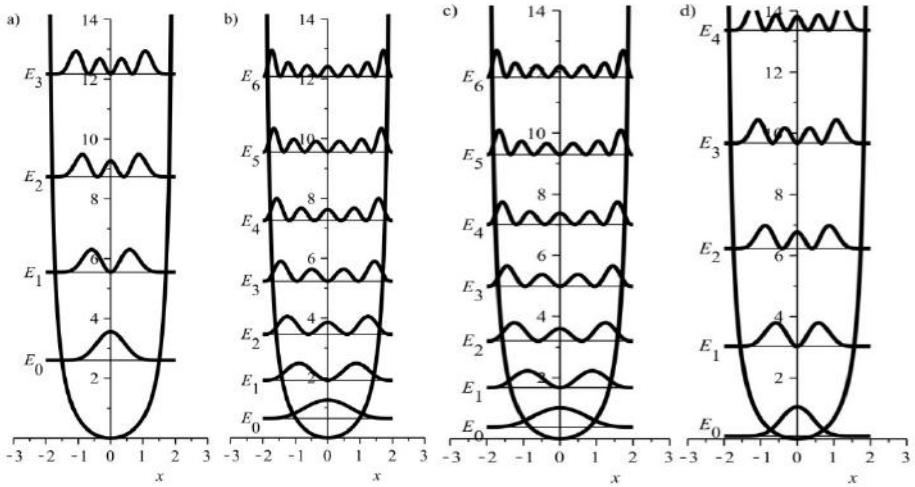

Fig. 1. Confined quantum harmonic oscillator potential (13) and behaviour of the corresponding non-equidistant energy levels (35) at value of the confinement parameter $a=2$ and probability densities $|\psi_n^{MB}(x)|^2$ of the ground and a) 3 excited states for value of the parameter $\alpha=-5$; b) 6 excited states for value of the parameter $\alpha=-0.5$; c) 6 excited states for value of the parameter $\alpha=-0.5$; d) 4 excited states for value of the parameter $\alpha=5$ ($m=\omega=\hbar=1$).

The limit between the confined and Hermite oscillators wavefunctions (36) and (8) is satisfied, too. Correctness of this limit is based on the existence of the following limit relation between Gegenbauer polynomials $C_n^{\bar{\lambda}}(x)$ and Hermite polynomials $H_n(x)$ [36]:

$$\lim_{a\to\infty}\bar{\lambda}^{-\frac{1}{2}n}C_n^{(\bar{\lambda}+\frac{1}{2})}\left(\frac{x}{\sqrt{\bar{\lambda}}}\right)=\frac{H_n(x)}{n!} \qquad (42)$$

Thanks to this limit relation, wavefunctions of the stationary states of the Morrow-Brownstein confined quantum harmonic oscillator with a position-dependent effective mass $\psi_n^{MB}(x)$ (36) reduce to wavefunctions of

the stationary states of the Hermite oscillator potential $\psi_n(x)$ (8) under the following limit relation:

$$\lim_{a\to\infty} \psi_n^{MB}(x) = \psi_n(x) \qquad (43)$$

Following asymptotics and limit relations can be useful during derivation of (43):

$$\Gamma_{|z|\to\infty} \simeq \sqrt{\frac{2\pi}{z}} e^{zlnz-z},$$

$$\Gamma\left(\sqrt{\bar{\lambda}^2+4\alpha^2}+1/2\right) \underset{\bar{\lambda}\to\infty}{\simeq} \sqrt{2\pi} e^{\bar{\lambda}ln\bar{\lambda}-\bar{\lambda}}, \bar{\lambda} = \frac{m\omega a^2}{\hbar},$$

$$\Gamma\left(n + 2\sqrt{\bar{\lambda}^2+4\alpha^2}+1\right) \underset{\bar{\lambda}\to\infty}{\simeq} 2^n \sqrt{4\pi\bar{\lambda}} e^{(2\bar{\lambda}+n)ln\bar{\lambda}-2\bar{\lambda}+2\bar{\lambda}ln2},$$

$$\lim_{\bar{\lambda}\to\infty} \bar{\lambda}^{\frac{n}{2}} c_n^{MB} = \tilde{c_0}\sqrt{\frac{n!}{2^n}}, \tilde{c_0} = \left(\frac{m\omega}{\pi\hbar}\right)^{\frac{1}{4}},$$

$$\lim_{\bar{\lambda}\to\infty} \left(1 - \frac{x^2}{a^2}\right)^{\frac{1}{2}\sqrt{\bar{\lambda}^2+4\alpha^2}} = e^{-\frac{m\omega x^2}{2\hbar}}$$

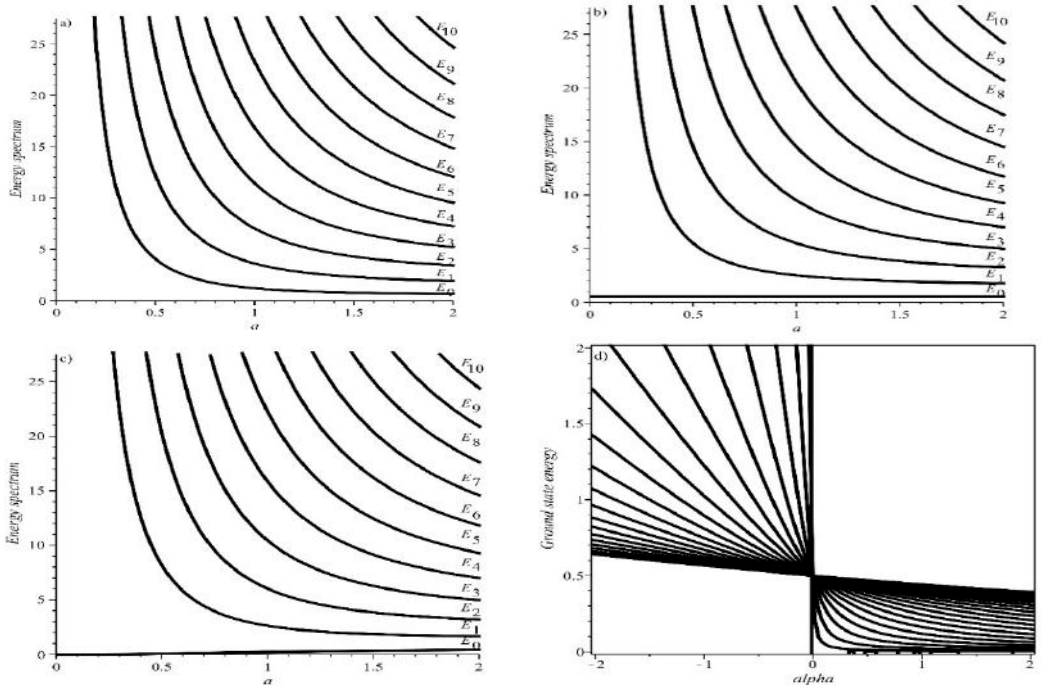

Fig. 2. Dependence of the non-equidistant energy levels (35) from the confinement parameter a for the ground and 10 excited states ($m = \omega = \hbar = 1$): a) $\alpha = -\frac{1}{2}$; b) $\alpha = 0$; c) $\alpha = \frac{1}{2}$; and d) dependence of ground state energy level from the α parameter for values of $a = 0.4$

In fig.1, we depicted confined quantum harmonic oscillator potential (13) and behaviour of the corresponding non-equidistant energy levels (35) at value of the confinement parameter $a = 2$ and probability densities $|\psi_n^{MB}(x)|^2$ of the ground and a) 3 excited states for value of the parameter $\alpha = -5$; b) 6 excited states for value of the parameter $\alpha = -0.5$; c) 6 excited states for value of the parameter $\alpha = 0.5$; d) 4 excited states for value of the parameter $\alpha = 5$ ($m = \omega = \hbar = 1$). Dependence of the non-equidistant energy levels (35) from the confinement parameter a for the ground and 10 excited states: a) $\alpha = -\frac{1}{2}$; b) $\alpha = 0$; c) $\alpha = \frac{1}{2}$; and d) dependence of ground state energy level from the α parameter for values of $a = 0.4$ are presented in fig.2 (all plots are depicted in $m = \omega = \hbar = 1$ system). Depicting dependence of the non-equidistant energy levels from the confinement

parameter a we observed that behaviour of the ground state for different values of α is completely different. Therefore, we decided to make a plot of the dependence of ground state energy level from parameter α for different values of the confinement parameter a. We observe that for some positive values of parameter α, ground state energy can reduce to zero. This happens due to existence of parameter α in both terms of the energy spectrum expression. In fig.1 we also observe how infinite high walls appear for harmonic oscillator depending on value of a and of course, we provide probability densities $|\psi_n^{MB}(x)|^2$ corresponding energy levels aiming to exhibit their behaviour within confinement effect. Due to that, we fix confinement parameter a in our plots at value $a = 2$, infinite walls also appear at values of position $x = \pm 2$.

One can extend this discussion, however, important point here is demonstration of exactly solubility of the quantum harmonic oscillator with Morrow-Brownstein kinetic energy operator under the confinement effect and obtaining explicit expressions of the wavefunctions of stationary states and energy spectrum through solution of the corresponding Schrödinger equation. Method applied here can be generalized further for one-dimensional relativistic confined oscillator systems, which also can exhibit surprising results both for physics and mathematics applications.

[1] *S.C. Bloch.* Introduction to Classical and Quantum Harmonic Oscillators. Wiley, New-York, 384 p.,1997.

[2] *S. Flügge.* Practical Quantum Mechanics: Vol I Springer, Berlin, 620 p., 1971.

[3] *Y. Ohnuki* and *S. Kamefuchi*. Quantum Field Theory and Parastatistics. Springer Verslag, New-York, 490 p., 1982).

[4] *N.M. Atakishiev, R.M. Mir-Kasimov* and *Sh.M.Nagiev*. Theor. Math. Phys.44, 592,1980.

[5] *M. Moshinsky* and *S. Szczepaniak.* J. Phys. A: Math. Gen.22, L817,1989.

[6] *S. Bruce* and *M. Minning.* Nuovu Cimento A 106,711,1993.

[7] *N.M. Atakishiev* and *S.K. Suslov*. Theor. Math. Phys.85, 1055,1990.

[8] *N.M. Atakishiyev, E.I. Jafarov, S.M. Nagiyev* and *K.B.Wolf. Rev.* Mex. Fis.44, 235,1998.

[9] *E.I. Jafarov, N.I. Stoilova* and *J. Van der Jeugt.* J. Phys. A: Math. Theor.44, 265203, 2011.*E.I. Jafarov, N.I.*

[10] *Stoilova* and *J. Van der Jeugt.* J. Phys. A: Math. Theor. 44, 355205, 2011.

[11] *E.I. Jafarov* and *J.Van der Jeugt.* J. Phys. A: Math. Theor. 45, 275301, 2012.

[12] *E.I. Jafarov, A.M. Jafarova* and *J.Van der Jeugt.* J. Phys. Conf. Ser. 597, 012047, 2015.

[13] *R. Oste* and *J. Van der Jeugt.* J. Phys. A: Math. Theor.49, 175204, 2016.

[14] *R. Oste* and *J. Van der Jeugt.* Phys. Atom. Nucl.80, 786, 2017.

[15] *E.I. Jafarov* and *J. Van der Jeugt*. J. Phys. A: Math. Theor.45, 485201, 2012.

[16] *F.C. Auluck.* Proc. Indian Nat. Sci. Acad.7, 133,1941.

[17] *S. Chandrasekhar.* Astrophys. J 97, 263,1943.

[18] *F.C. Auluck* and *D.S. Kothari.* Math. Proc. Camb. Phil. Soc.41, 175,1945.

[19] *A. Consortini* and *B.R. Frieden*. Nuovo Cim. B 35, 153,1976.

[20] *F.C. Rotbart.* J. Phys. A: Math. Gen. 11, 2363,1978.

[21] *A.H. MacDonald* and *P. Středa.* Phys. Rev. B 29, 1616, 1984.

[22] *M. Grinberg, W. Jaskólski, Cz. Coepke, J.Planelles* and *M.Janowicz.* Phys. Rev. B 50, 6504, 1994.

[23] *Lj. Stevanović* and *K.D. Sen.* J. Phys. B: At. Mol. Opt. Phys. 41, 225002, 2008.

[24] *W.A. Harrison.* Phys. Rev. 123, 85, 1961.

[25] *I. Giaever.* Phys. Rev. Lett.5, 147, 1960.

[26] *I. Giaever.* Phys. Rev. Lett.5, 464,1960.

[27] *D. J. BenDaniel* and *C.B.Duke.* Phys. Rev.152, 683,1966.

[28] *Q-G. Zhu* and *H. Kroemer*. Phys. Rev. B27 3519, 1983.

[29] *R.A. Morrow* and *K.R. Brownstein.* Phys. Rev. B 30, 678, 1984.

[30] *R.A. Morrow.* Phys. Rev. B 35, 8074,1987.

[31] *G.X. Ju, Ch.Y. Cai, Y. Xiang* and *Zh.Zh. Ren.* Commun. Theor. Phys. 47, 1001, 2007.

[32] *G.X. Ju, Ch.Y. Cai* and *Zh.Zh. Ren.* Commun. Theor. Phys. 51, 797, 2009.

[33] *N. Amir* and *Sh. Iqbal. Commun.* Theor. Phys. 62, 790, 2014.

[34] *M.K. Bahar* and *S. Yasuk.* Canadian J. Phys. 91, 191, 2013.

[35] *M. K. Bahar* and *S.Yasuk.* Canadian J. Phys. 92, 1565, 2014.

[36] *R. Koekoek, P.A. Lesky* and *R.F. Swarttouw.* Hypergeometric orthogonal polynomials and their q-analogues. Springer Verslag, Berlin, 578p., 2010.

[37] *F. Nikiforov* and *V.B. Uvarov.* Special Functions of Mathematical Physics: A Unified Introduction with Applications. Birkhauser, Basel, 427p., 1988.

Received: 14.07.2021

DYNAMICS OF $S = \frac{1}{2}$ AND $S = 1$ ISING SPIN SYSTEM IN RESTANGULAR NANOWIRE

V.A. TANRIVERDIYEV, V.S. TAGIYEV
Institute of Physics of the National Academy of Sciences of Azerbaijan,
H.Javid ave.131, Baku AZ 1143
E-mail: vahid_tanriverdi @yahoo.com

The dynamic behaviors are studied, within a mean-field approach, in the kinetic mixed spin (1/2, 1) Ising nanowire system with core-shell structure under the presence of a time varying (cosinusoidal) magnetic field by using the Glauber-type stochastic dynamics. The time variations of the average shell and core magnetizations are investigated to obtain the phases in the system. In order to determine the behaviors of time variotions of the average magnetization, the stationary solutions of the dynamic effective filed coupled equations have been studied for various values of interaction parameters, temperature and external magnetic field. It has been determined that the system contain paramagnetic (*p*), ferrimagnetic (*i)*, nonmagnetic (*nm*) phases, and also coexistence regions, which strongly depend on interaction parameters.

Keywords: Nanowire; Ising model; Mixed spin system; Mean-field approach; Glauber-type stochasticdynamic.
PASC: 75.70. AK.

1. INTRODUCTION

Researchers have made great efforts analytically [1], experimentally [2] and computer simulations [3] to provide a better understanding of the magnetic behavior of nanowires. Theoretically, the Ising model with a core /shell structure has been accepted in the literature to explain many characteristic phenomena in magnetic nanomaterials, such as magnetic nanoparticles, nanotubes and nanowires, and has begun to be applied in many fields [4-9]. Moreover, the magnetic behaviors of various magnetic nanowires have been investigated in detail using mean field approach [10], correlated effective field theory [11], Green function formalism [12], Bethe Peierls approach [13], Monte Carlo simulation (MCS) [14] and others statistical physics methods. More recently, Boughrara et al. [15] investigated the phase diagrams and magnetic behaviors of the mixed spin (1/2, 1) Ising nanowire and obtained phase diagrams that displayed very rich critical behaviors, such as first-, second-order phase transitions, compensation temperatures, depending on the interaction parameters. Albayrak [16] studied the Ising nanowire system with core-shell structure mixed spin (1/2, 1) in the Bethe weave, and the resulting phase diagrams showed first-, second-order phase transitions and triple critical point behavior.

Although enough studies have been done to understand the balance properties of nanostructured systems using the Ising model, there have not been enough studies for its dynamic properties and especially in recent years, the dynamic properties of these nanostructured systems have been started to be studied. Dynamic phase transitions of cylindrical Ising nanowires under the oscillating outer magnetic field for the ferromagnetic and antiferromagnetic interaction parameters were investigated using Glauber-type stochastic dynamic based effective field theory [17-19].

In this paper, the dynamic behavior of the mixed spin (1/2, 1) Ising nanowire system will be examined using the mean-area dynamic and Glauber-type stochastic dynamic. In order to find the phases, present in the system, time dependent behaviors of the average order parameters will be examined. Thus, it will be possible to interpret dynamic phase transitions and dynamic phase diagrams of the mixed spin (1/2, 1) Ising nanowire system, which is one of the main objectives of this paper.

2. DESCRIPTION OF THE METHOD AND MODEL

Glauber-type stochastic dynamic based mean field approach method is used to investigate the dynamic magnetic behavior of complex spin systems such as ferrimagnetic mixed spin (1/2, 1) Ising nanowire. The schematic representation with rectangular structure that will be used in this paper is given in figure 1.

The model of interest is alternatively composed of three repetitive substrates, *A*, *B* and *C*. The first substrate *A*, belonging to the spin-1/2 magnetic atoms in the core, takes the values of ± 1/2. The other two substrates *B* and *C*, take the values of ± 1, 0, and the *S* spins in the shell take the values of spin-1. The core of the core is occupied by the σ spins, while the shell is surrounded by the *S* spins. Hamiltonian expression of the cylindrical mixed spin (1/2, 1) Ising nanowire system, which includes the closest neighbor interactions, the term crystalline or single ion anisotropy, and the term dependent outer magnetic field is defined as

$$H = -J \sum_{<ij>} \sigma_i \sigma_j - J \sum_{<im>} \sigma_i S_m \; - \; J_s \sum_{<mn>} S_m S_n - \mathrm{D} \sum_{<m>} S_m^2 + \mathrm{h(t)} \left(\sum_{<i>} \sigma_i + \sum_{<m>} S_m \right) \quad (1)$$

131, H.Javid ave, AZ-1143, Baku
ANAS, Institute of Physics
E-mail: jophphysics@gmail.com

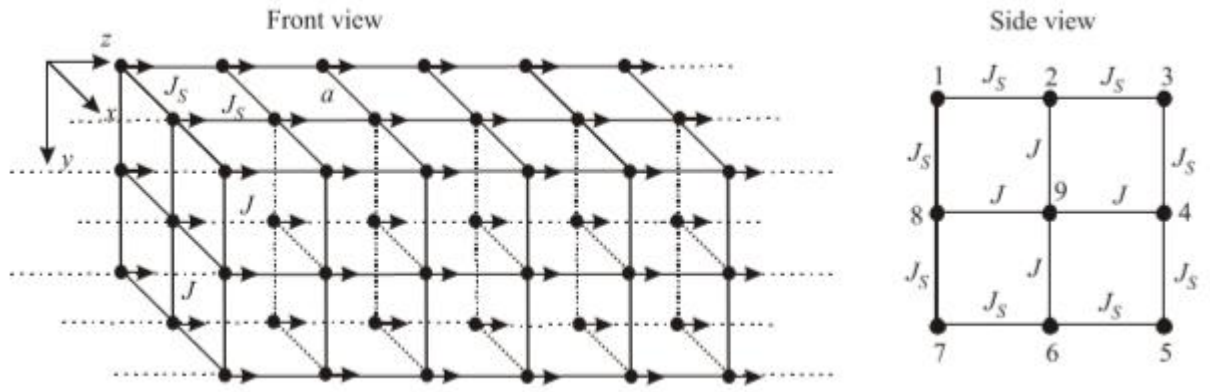

Fig. 1. Model of simple cubic rectangular nanowires. The nanowires are infinite in the direction to the axes z

where $\sigma = \pm 1/2, \quad S = \pm 1, 0$. The sum of $< ij >$, $< im >$ and $< mn >$ means that the adjacent spins between the core, core-shell, and at the shell surface. J is the exchange coupling between spins labeled 9 and its nearest neighbors, and J_s is that between surface spins. D denotes the crystal-field or single-ion anisotropy interaction term, and $h(t) = h_0 cos\omega t$ is the time-dependent oscillating external magnetic field. Since the atoms on the surface of the shell have a great influence on the physical properties of nanostructured materials, the term of the bi-linear interaction between magnetic atoms on the surface of the nanostructured materials is defined as follows $J_s = J(1 + \Delta_s)$.

In the presence of time-dependent oscillating external magnetic, we will use the Glauber dynamics and use the Master equation to obtain the mean-field dynamic equations describing the dynamic behavior of the system for the mixed spin (1/2, 1) Ising nanowire system. The mixed spin (1/2, 1) Ising nanowire system changes at a rate of 1 / τ per unit time according to the Glauber-type stochastic dynamic. When the spins in the substrates B and C remain constant, at time t, the probability function when the system has the spin configuration $\sigma_1, \sigma_2, \dots, \sigma_j, .., \sigma_N$ is defined by $P^A(\sigma_1, \sigma_2, \dots, \sigma_j, .., \sigma_N, t)$. When the spins on the A and C substrates remain constant, the probability function at time t of the system when it has the spin configuration $S_1, S_2, \dots, S_j, .., S_N$ is defined by $P^B(S_1, S_2, \dots, S_j, .., S_N, t)$. Finally, when the spins on the substrates A and B remain constant, the probability function at time t of the system is defined by $P^C(S_1, S_2, \dots, S_j, .., S_N, t)$.

Considering that the spins in the B and C substrates are fixed for a moment, the master equation for the substrates A is writen as

$$\frac{d}{dt}P^A(\sigma_1, \sigma_2, \dots, \sigma_j, .., \sigma_N, t) = -\sum_j \left(w_j(\sigma_j \to -\sigma_j)\right) P^A(\sigma_1, \sigma_2, \dots, \sigma_j, .., \sigma_N, t) + \\ +\sum_j \left(w_j(-\sigma_j \to \sigma_j) P^A(\sigma_1, \sigma_2, \dots, -\sigma_j, .., \sigma_N, t)\right) \quad (2)$$

Here $w_j(\sigma_j \to -\sigma_j)$ is the probability that the spin of ith will change from σ_j state to $-\sigma_j$ state per unit time. Using the canonical set probability distribution expression probability $w_j(\sigma_j \to -\sigma_j)$ can be written as

$$w_j(\sigma_j \to -\sigma_j) = \frac{1}{\tau}\frac{\exp[-\beta\Delta E(\sigma_j \to -\sigma_j)]}{\exp[-\beta\Delta E(\sigma_j \to -\sigma_j)]+1} \quad (3)$$

Here, $\beta = 1/k_B T$, T is the absolute temperature and k_B is the Boltzmann constant. The change in energy corresponding to following situation

$$\Delta E(\sigma_j \to -\sigma_j) = E(-\sigma_j) - E(\sigma_j) = 2\sigma_j x$$

$$\Delta E(-\sigma_j \to \sigma_j) = E(\sigma_j) - E(-\sigma_j) = -2\sigma_j x$$

where

$$x = 2J < \sigma_j > +4J \sum_{<i,j>} S_i + h(t)$$

If these energy change expressions found are substituted in the equation (3), $w_j(\sigma_j \to -\sigma_j)$ probability densities

$$w_j\left(\frac{1}{2} \to -\frac{1}{2}\right) = \frac{1}{2\tau}\frac{\exp[-\beta x/2)]}{\cosh[\beta x/2)]} \quad (4a)$$

$$w_j\left(-\frac{1}{2} \to \frac{1}{2}\right) = \frac{1}{2\tau}\frac{\exp[\beta x/2)]}{\cosh[\beta x/2)]} \quad (4b)$$

Using the master equation, the general average-area dynamic equation for sub-A is obtained as follows:

$$\tau\frac{d}{dt} < \sigma_j > = - < \sigma_j > + \frac{1}{2}\tanh[\beta\, x/2)] \quad (5)$$

If we make substitutions $m_c = < \sigma_j >_A$, $m_{s1} = < S_j >_B$, $\Omega = \tau\omega$ and $\xi = \omega t$, then we can write equation (5) as follows

$$\Omega \frac{d}{d\xi} m_c = -m_c + \frac{1}{2}\tanh\left[\beta\left(2Jm_c + 4Jm_{s1} + h(\xi)\right)/2\right] \tag{6}$$

In the mixed spin (1/2, 1) Ising nanowire system, considering the spin in the *A* and *C* substrates remains constant for one, we can also obtain the average area dynamic equations for the *B* substrate using similar calculations as below. In this case, the master equation for *B* substrate

$$\frac{d}{dt} P^B\left(S_1, S_2, \dots, S_j, .., S_N, t\right) = -\sum_j \sum_{S_j \neq S_j'} w_j^B\left(S_j \to S_j'\right) P^B(S_1, S_2, \dots, S_j, .., S_N, t) + \\ + \sum_j \sum_{S_j \neq S_j'} w_j^B\left(S_j' \to S_j\right)\ P^B(S_1, S_2, \dots, S_j', .., S_N, t) \tag{7}$$

While the system is in balance, with the help of the master equation and general definition of the canonical distribution, the probability of each spin to pass from S_j to S_j' per unit time

$$w_j^B\left(S_j \to S_j'\right) = \frac{\exp[-\beta \Delta E^B(S_j \to S_j')]}{\tau \sum_{S_j'} \exp[-\beta \Delta E^B(S_j \to S_j')]} \tag{8}$$

Then the expression of $\Delta E^B(S_j \to S_j')$ is found by using the Hamiltonian expression:

$$\Delta E^B\left(S_j \to S_j'\right) = -\left(S_j' - S_j\right)\left(J \sum_{<i,j>} \sigma_i + J_s \sum_{<i,j>} S_i + h(t)\right) - D\left({S_j'}^2 - {S_j}^2\right) \tag{9}$$

If these energy change expressions found are substituted in the equation (8), probability densities for each *Sj* state are obtained as follows.

$$w_j^B(1 \to 0) = w_j^B(-1 \to 0) = \frac{\exp[-\beta D]}{\tau(\exp[-\beta D] + 2\cosh[\beta y])}$$

$$w_j^B(-1 \to 1) = w_j^B(0 \to 1) = \frac{\exp[\beta y]}{\tau(\exp[-\beta D] + 2\cosh[\beta y])}$$

$$w_j^B(0 \to -1) = w_j^B(1 \to -1) = \frac{\exp[-\beta y]}{\tau(\exp[-\beta D] + 2\cosh[\beta y])}$$

where $y = J \sum_{<i,j>} \sigma_i + J_s \sum_{<i,j>} S_i + h(t)$

If the mean-area approach is used, the mean-area dynamic equation for the *B* substrate,

$$\Omega \frac{d}{d\xi} m_{s1} = -m_{s1} + \frac{2\sinh\left[\beta\left(Jm_c + 2J_s m_{s1} + 2J_s m_{s2} + h(\xi)\right)\right]}{\exp[-\beta D] + 2\cosh\left[\beta\left(Jm_c + 2J_s m_{s1} + 2J_s m_{s2} + h(\xi)\right)\right]} \tag{10}$$

Similar to the equation (10), the following equation can be obtained for the *t C* substrate

$$\Omega \frac{d}{d\xi} m_{s2} = -m_{s2} + \frac{2\sinh\left[\beta\left(2J_s m_{s1} + 2J_s m_{s2} + h(\xi)\right)\right]}{\exp[-\beta D] + 2\cosh\left[\beta\left(2J_s m_{s1} + 2J_s m_{s2} + h(\xi)\right)\right]} \tag{11}$$

3. NUMERICAL RESULTS AND DISCUSSION

In order to find the phases, present in the system, the stable solutions of the mean-field dynamical equations given by equation (6), (10) and (11) will be examined for different crystal field *(d)*, magnetic field amplitude *(h)* and temperature *(T)* values. The stationary solutions of equations (6), (10) and (11) are a periodic function of ξ for the period 2π of a periodic function, so it will be, so $m_c(\xi) = m_c(\xi + 2\pi)$, $m_{s1}(\xi) = m_{s1}(\xi + 2\pi)$ and $m_{s2}(\xi) = m_{s2}(\xi + 2\pi)$. Moreover, they can be one of the three types according to whether they have or not have the properties

$$m_c(\xi + \pi) = -m_c(\xi) \tag{11a}$$

$$m_{s1}(\xi + \pi) = -m_{s1}(\xi) \tag{11b}$$

and

$$m_{s2}(\xi+\pi) = -m_{s2}(\xi) \qquad (11c)$$

The first type solution of equation (11a) here is called the symmetric solution, and this solution corresponds to the irregular or paramagnetic *(p)* solution. In this solution, the average order parameters, namely the average sublattice magnetizations m_c, m_{s1} and m_{s2} are equal to each other and oscillate around the zero value, conforming to the external magnetic field. The second type of solution does not fit the equation given by (11a), but obeys the equations given by (11b) and (11c). This solution corresponds to the non-magnetic (nm) solution and oscillates around $m_c = \pm 1/2$ values in this solution, while m_{s1} and m_{s2} oscillates around zero. In the third type of solution, the solution we obtained does not obey equations (11) and this is the unsymmetrical solution, which corresponds to the ferrimagnetic *(i)* solution. In this solution, m_c, m_{s1} and m_{s2} are not equal and they oscillate around non-zero values, i.e. $m_c = \pm 1/2$ and $m_{s1(2)} = \pm 1$ and do not conform to the external magnetic field. These solutions are clearly seen by numerically solving the mean-area dynamic equations given by (6), (10) and (11). These equations are solved for the given parameters and initial values, besides paramagnetic (p), non-magnetic *(nm)* and ferrimagnetic (i) base phases in the system *i+ nm*, *nm + p*, *i+nm +p* and *i+p* mixed phases were found. Some solutions corresponding to these phases are shown in figure 2.

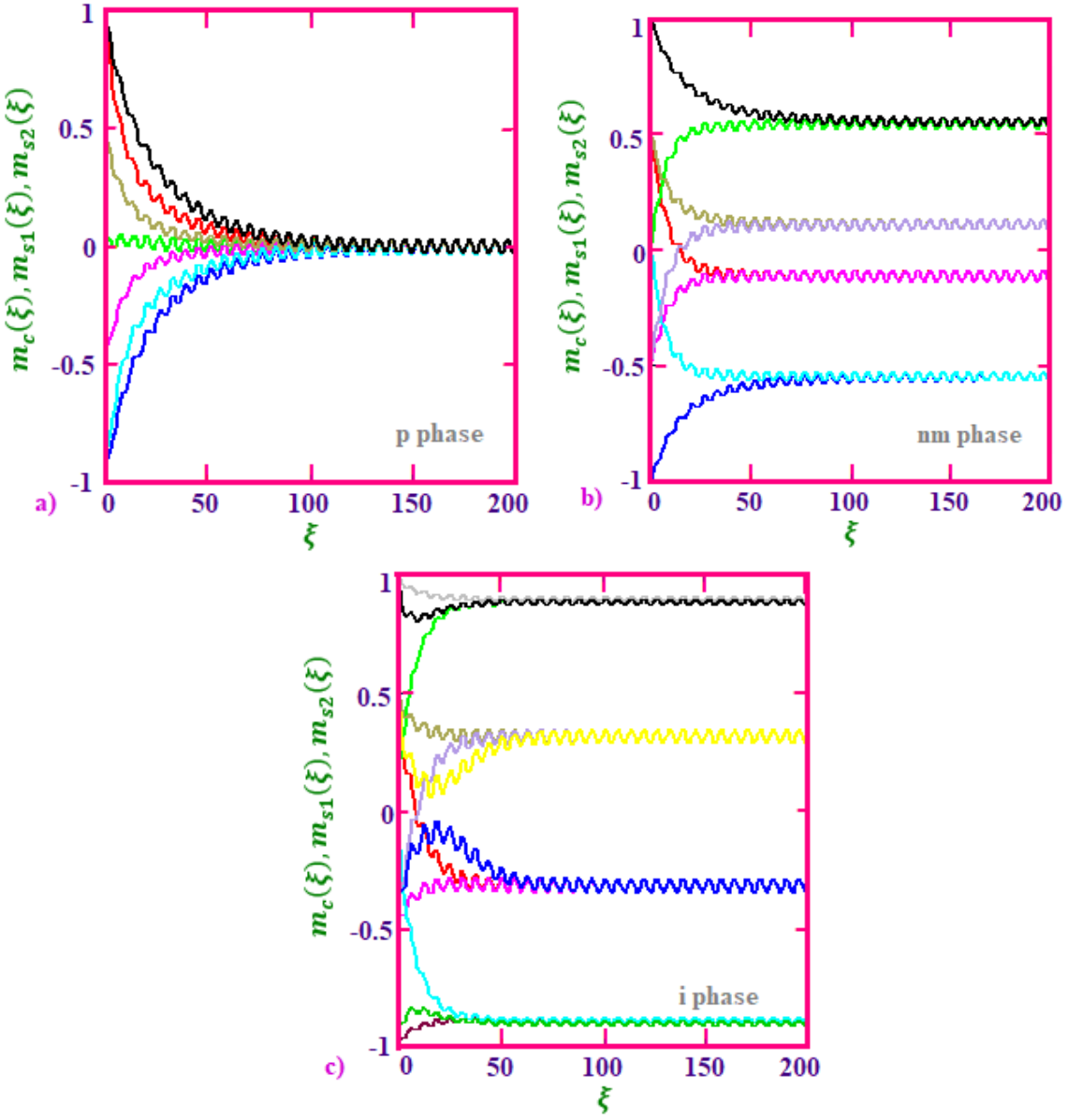

Fig. 2. Time variations of the core and shell magnetizations:
a) paramagnetic phase $k_BT/J = 5.8$, $h_0/J = 1.6$, $J_s/J = 1.8$, $D/J = -1$;
b) nonmagnetic phase $k_BT/J = 5.2$, $h_0/J = 1.6$, $J_s/J = 2.4$, $D/J = -1$;
c) ferrimagnetic phase $k_BT/J = 2.4$, $h_0/J = 1.6$, $J_s/J = 1.8$, $D/J = -1$;

[1] *W.T. Coffey, D.S.F. Crothers, J.L. Dormann, Y.P.Kalmykov, E.C. Kennedey, W.Wernsdorfer*. Phys. Rev. Lett. 80, 5655. 37, 1998.
[2] *S. Momose, H. Kodama, T. Uzumaki, A. Tanaka.* Appl. Phys. Lett. 85, 1748, 2004.
[3] *M. Vasilakaki, K.N. Trohidou*. Phys.Rev. B 79, 144402, 2009.
[4] *A.F. Bakuzis, P.C. Morais. J*. Magn. Magn. Mater. 285, 145-154, 2005.
[5] *T. Kaneyoshi*. J. Magn. Magn. Mater., 321, 3430-3435, 2009.
[6] *M. Vasilakaki, K.N. Trohidou.* Phys.Rev. B 79, 144402, 2009.
[7] *T. Kaneyoshi*. Phys.Status Solidi., B 248, 250-258, 38, 2011.
[8] *O. Canko, A. Erdinç, F. Taskin, A.F. Yildirim.* J.Magn. Magn. Mater. 324, 508-513, 2012.
[9] *U. Akıncı.* J. Magn. Magn. Mater., 324, 3951-3960, 2012.
[10] *V.S. Leite, B.C.S. Grandi, W. Figueiredo.* Phys. Rev. B 74, 094408, 2006.
[11] *T. Kaneyoshi.* Physica B 414, 72, 2013.
[12] *K.R. Heim, G.G. Hembree, K.E. Schmidt, M.R. Scheinfein.* Appl. Phys. Lett. 67, 2878, 1995.
[13] *L.G.C. Rego, W. Figueiredo.* Phys. Rev. B 64, 144424, 2001.
[14] *H. Magoussi, A. Zaim, M. Kerouad.* Solid State Commun. 200, 32-41, 2014.
[15] *E. Albayrak.* J. Magn. Magn. Mater., 401, 532-538, 2016.
[16] *M. Keskin, M. Ertas, O. Canko.* Phys. Scr., 79, 025501, 2009.
[17] *B. Deviren, M. Keskin, O. Canko.* J. Magn. Magn. Mater., 321, 458-466, 2009.
[18] *B. Deviren, M. Keskin.* J. Stat. Phys., 140, 934-947, 2010.

Received: 17.07.2021

ON THE EXACT SOLUTION OF THE CONFINED POSITION-DEPENDENT MASS HARMONIC OSCILLATOR MODEL WITH THE KINETIC ENERGY OPERATOR COMPATIBLE WITH GALILEAN INVARIANCE UNDER THE HOMOGENEOUS GRAVITATIONAL FIELD

A.M. MAMMADOVA
Institute of Physics, Azerbaijan National Academy of Sciences
H. Javid av. 131, AZ1143, Baku, Azerbaijan
E-mail: a.mammadova@physics.science.az

Exactly-solvable confined model of the quantum harmonic oscillator under the external gravitational field is studied. Confinement effect is achieved thanks to the effective mass changing with position. Nikiforov-Uvarov method is applied for solving exactly corresponding Schrödinger equation. Analytical expressions of the wavefunctions of the stationary states and energy spectrum are obtained.

Keywords: Harmonic oscillator, gravitational field, position-dependent mass.
PACS: 03.65.-w, 02.30 Hq.03.65.Ge

1. INTRODUCTION

Quantum systems with position-dependent effective mass have been the subject of many attracting studies in recent years [1-4]. The Schrödinger equation corresponding to such systems with non-constant mass provides interesting and useful solutions for the description of them. At the same time, behavior of the quantum system influenced from attached external field is also within the attraction of the scientists working on this and related research topics [5,6]. Main reason is that external field attached to the quantum system under consideration can thoroughly change its main properties. Then, such an effect also can open for studying many of previously hidden aspects regarding them.

In present paper, we study an oscillator model that is under the influence of the external homogeneous gravitational field. Already, same model exhibiting confinement effect was studied in detail and results have been published in [7]. Then, taking into account importance of the appearance of the external field, we decided to obtain more general solutions by extending free motion in the confined oscillator potential to the similar motion, but through taking into account external homogeneous gravitational field. We are able to obtain analytical expressions of the wavefunctions corresponding to our model under study as well as its energy spectrum. In our studies, we preserved general definition of the kinetic operator, which is still compatible with the Galilean invariance. Correctness of the obtained analytical expressions is proven via their correct reduce to the known non-relativistic results under the certain limit relations.

We structured our paper as follows: in Section 2, basic known information is provided for the non-relativistic quantum harmonic oscillator. Briefly, analytical solutions of the Schrödinger equation for it are presented within the canonical approach. Analytical solutions cover both wave functions of the stationary states of the quantum oscillator itself as well as same model but under the external homogeneous gravitational field. It is shown that both wave functions are expressed via the Hermite polynomials, but wave function for the model suppressed to the external homogeneous gravitational field differs from free harmonic oscillator with the shifted position x. Analytical expressions of the energy spectrum of both models also have similar behavior – both of them are equidistant. However, energy spectrum of the model under the external homogeneous gravitational field differs with some shifted constant parameter that appears as a result of the applied external field. It is shown that analytical expression of the wave functions and energy spectrum of the model with an applied external homogeneous gravitational field easily recovers the model of the non-relativistic oscillator within the canonical approach for case of the disappearance of the external field. Section 3 is devoted to the confined position-dependent mass harmonic oscillator model under the homogeneous gravitational field. In order achieve the confinement effect, we replaced constant effective mass of the model under study with the effective mass that varies with position x. Then, aiming to preserve Hermiticity property of the Hamiltonian of the model, we also replaced its kinetic energy operator with the kinetic energy operator compatible with Galilean invariance. Both analytical expressions of the wave functions and energy spectrum of the confined position-dependent mass harmonic oscillator model with the kinetic energy operator compatible with Galilean invariance and same model but under the homogeneous gravitational field are presented here. Final section contains some brief discussions and possible limit relations between the models presented here.

2. NON-RELATIVISTIC QUANTUM HARMONIC OSCILLATOR WITHIN THE CANONICAL APPROACH – EXACT SOLUTIONS THE MODEL WITH BOTH CASES OF ABSENCE AND EXISTENCE

131, H.Javid ave, AZ-1143, Baku
ANAS, Institute of Physics
E-mail: jophphysics@gmail.com

OF THE EXTERNAL GRAVITATIONAL FIELD $V(x) = m_0 g x$

Quantum-mechanical solution for the one-dimentional harmonic oscillator with wavefunctions, which have to vanish at infinity can be obtained by solving exactly one-dimensional stationary Schrödinger equation in the position representation

$$\left[\frac{\hat{p}_x^2}{2m} + V(x)\right]\psi(x) = E\psi(x), \quad (2.1)$$

with non-relativistic harmonic oscillator potential

$$V(x) = \frac{m_0\omega^2 x^2}{2}. \quad (2.2)$$

Here, m_0 and ω are constant effective mass and angular frequency of the non-relativistic quantum harmonic oscillator, and one-dimentional momentum operator $\hat{p}_x$ is defined in canonical approach as

$$\hat{p}_x = -i\hbar\frac{d}{dx}. \quad (2.3)$$

Taking into account (2.2) and (2.3) in (2.1) we have

$$\frac{d^2\psi}{dx^2} + \frac{2m_0}{\hbar^2}\left(E - \frac{m_0\omega^2 x^2}{2}\right)\psi = 0. \quad (2.4)$$

Solving this equation exactly, we obtain the following expression for the energy spectrum:

$$E \equiv E_n = \hbar\omega\left(n + \frac{1}{2}\right), \quad n = 0,1,2, \ldots \quad (2.5).$$

It is possible also to show that wavefunctions of the stationary states the model under consideration in the position representation obtained from (2.4) are

$$\psi \equiv \psi_n(x) = \frac{1}{\sqrt{2^n n!}}\left(\frac{m_0\omega}{\pi\hbar}\right)^{\frac{1}{4}} e^{-\frac{m\omega x^2}{2\hbar}} H_n\left(\sqrt{\frac{m_0\omega}{\hbar}}x\right), \quad (2.6)$$

where $H_n(x)$ are Hermite polynomials defined in terms of hypergeometric function as follows

$$H_n(x) = (2x)^n {}_2F_0\left(-\frac{n}{2}, -\frac{n-1}{2}; \frac{1}{x^2}\right). \quad (2.7)$$

Let's now consider the model of a linear harmonic oscillator (2.2) in external homogeneous gravitational field. Then, the potential of the harmonic oscillator is

$$V(x) = \frac{m_0\omega^2 x^2}{2} + m_0 g x. \quad (2.8)$$

Now we need to solve the following Schrödinger equation:

$$\left[\frac{\hat{p}_x^2}{2m_0} + \frac{m_0\omega^2 x^2}{2} + m_0 g x\right]\psi(x) = E\psi(x). \quad (2.9)$$

Note that all calculations are still in a canonical approach. Therefore, one-dimensional momentum operator can be written as (2.3). We have

$$\frac{d^2\psi}{dx^2} + \left[\frac{2m_0 E}{\hbar^2} - \frac{{m_0}^2\omega^2}{\hbar^2}(x + x_0)^2 + \frac{g^2}{\omega^4}\right]\psi = 0, \quad (2.10)$$

where,

$$x_0 = \frac{g}{\omega^2}. \quad (2.11)$$

We can rewrite (2.10) as

$$\frac{d^2\psi}{dx^2} + \left[\frac{2m_0\tilde{E}}{\hbar^2} - \frac{{m_0}^2\omega^2}{\hbar^2}(x + x_0)^2\right]\psi = 0, \quad (2.12)$$

$$\tilde{E} = E + \frac{\hbar^2 g^2}{2m_0\omega^4}. \quad (2.13)$$

Analytical solution of the equation (2.12) leads to explicit expression of the discrete equidistant energy spectrum:

$$E \equiv E_n^g = \hbar\omega\left(n + \frac{1}{2}\right) - \frac{\hbar^2 g^2}{2m_0\omega^4}, \; n = 0,1,2, \ldots. \quad (2.14)$$

The corresponding wavefunctions are

$$\psi \equiv \psi_n^g(x) = \frac{1}{\sqrt{2^n n!}}\left(\frac{m_0\omega}{\pi\hbar}\right)^{\frac{1}{4}} e^{-\frac{m_0\omega\left(x+\frac{g}{\omega^2}\right)^2}{2\hbar}} H_n\left(\sqrt{\frac{m_0\omega}{\hbar}}\left(x+\frac{g}{\omega^2}\right)\right). \tag{2.15}$$

One easily observes that

$$\psi_n^g(x) = \psi_n(x - x_0).$$

Under the case $g = 0$ both energy spectrum E_n^g (2.14) and wavefunctions $\psi_n^g(x)$ (2.15) correctly recover energy spectrum E_n (2.5) and wavefunctions $\psi_n(x)$ (2.6).

3. CONFINED POSITION-DEPENDENT MASS HARMONIC OSCILLATOR MODEL UNDER THE HOMOGENEOUS GRAVITATIONAL FIELD

Recently, we considered the quantum harmonic oscillator problem confined in the finite region, which effective mass varied with position $m_0 \to M(x)$ and its kinetic energy operator was compatible with Galilean invariance [8]:

$$\widehat{H}_0^{GI} = -\frac{\hbar^2}{6}\left[\frac{1}{M(x)}\frac{d^2}{dx^2} + \frac{d}{dx}\frac{1}{M(x)}\frac{d}{dx} + \frac{d^2}{dx^2}\frac{1}{M(x)}\right]. \tag{3.1}$$

We introduced confined harmonic oscillator potential as

$$V(x) = \begin{cases} \frac{M(x)\omega^2x^2}{2}, & |x| < a, \\ \infty, & |x| \geq a, \end{cases} \tag{3.2}$$

and then solved exactly the Schrödinger equation corrsponding to the following Galilean invariant Hamiltonian:

$$\widehat{H}^{GI} = -\frac{\hbar^2}{2M}\left[\frac{d^2}{dx^2} - \frac{M'}{M}\frac{d}{dx} - \frac{1}{3}\frac{M''}{M} + \frac{2}{3}\left(\frac{M'}{M}\right)^2\right] + \frac{M(x)\omega^2x^2}{2}. \tag{3.3}$$

Here, we also defined position-dependent effective mass $M(x)$ via the following analytical expression:

$$M \equiv M(x) = \frac{a^2m_0}{a^2-x^2}. \tag{3.4}$$

We obtained that energy spectrum E_n^{GI} is non-equidistant and has the following expression:

$$E_n^{GI} = \hbar\omega\left(n+\frac{1}{2}\right) + \frac{\hbar^2}{2m_0a^2}n(n+1) + \frac{\hbar^2}{3m_0a^2}, \tag{3.5}$$

whereas the wavefunctions of the stationary states ψ^{GI} are expressed through the Gegenbauer polynomials by the following manner:

$$\tilde{\psi}^{GI}(x) = c_n^{GI}\left(1-\frac{x^2}{a^2}\right)^{\frac{m_0\omega a^2}{2\hbar}} C_n^{\left(\frac{m_0\omega a^2}{\hbar}+\frac{1}{2}\right)}\left(\frac{x}{a}\right). \tag{3.6}$$

Here, Gegenbauer polynomials $C_n^{\bar{\lambda}}(x)$ are defined in terms of the ${}_2F_1$ hypergeometric functions as follows:

$$C_n^{(\bar{\lambda})}(x) = \frac{(2\bar{\lambda})_n}{n!} \quad {}_2F_1\left(\begin{matrix}-n, n+2\bar{\lambda} \\ \bar{\lambda}+\frac{1}{2}\end{matrix};\ \frac{1-x}{2}\right),\ \bar{\lambda} \neq 0.$$

*N*ormalization factor c_n^{GI} is obtained from the orthogonality relation for the Gegenbauer polynomials and its exact expression is the following:

$$c_n^{GI} = 2^{\frac{m_0\omega a^2}{\hbar}}\Gamma\left(\frac{m_0\omega a^2}{\hbar}+\frac{1}{2}\right)\sqrt{\frac{\left(n+\frac{m_0\omega a^2}{\hbar}+\frac{1}{2}\right)n!}{\pi a\Gamma\left(n+\frac{2m_0\omega a^2}{\hbar}+1\right)}}.$$

Now we can explore confined position-dependent mass harmonic oscillator model under the homogeneous gravitational field. First of all, we introduce external field to confined harmonic oscillator potential (3.2) as follows:

$$V(x)=\begin{cases}\frac{M(x)\omega^2x^2}{2}+M(x)gx, & |x|\le a,\\ \infty, & |x|>a.\end{cases} \tag{3.7}$$

Taking into account analytical definition of the position-dependent effective mass $M(x)$ (3.4) we need to solve the following Schrödinger equation:

$$\left[\frac{d^2}{dx^2}-\frac{2x}{a^2-x^2}\frac{d}{dx}+\frac{2}{3}\frac{4x^2}{(a^2-x^2)^2}-\frac{1}{3}\frac{2}{a^2-x^2}-\frac{1}{3}\frac{8x^2}{(a^2-x^2)^2}\right]\psi+\frac{2M}{\hbar^2}\left[E-\frac{M\omega^2x^2}{2}-Mgx\right]\psi=0 \tag{3.8}$$

Introduction of the new dimensionless variable ξ as:

$$\xi=\frac{x}{a},\quad \frac{d}{dx}=\frac{1}{a}\frac{d}{d\xi},\quad \frac{d^2}{dx^2}=\frac{1}{a^2}\frac{d^2}{d\xi^2}$$

and

$$c_0=\frac{2m_0a^2E}{\hbar^2},\quad c_1=\frac{2{m_0}^2ga^3}{\hbar^2},\quad c_2=c_0+{\lambda_0}^4a^4,$$

leads to:

$$\psi''-\frac{2\xi}{1-\xi^2}\psi'+\left(\frac{c_0}{1-\xi^2}-\frac{(c_2-c_0)\xi^2}{(1-\xi^2)^2}-\frac{2}{3}\frac{1}{1-\xi^2}-\frac{c_1\xi}{(1-\xi^2)^2}\right)\psi=0.$$

Taking into account

$$\frac{c_0}{1-\xi^2}-\frac{(c_2-c_0)\xi^2}{(1-\xi^2)^2}-\frac{2}{3}\frac{1}{1-\xi^2}-\frac{c_1\xi}{(1-\xi^2)^2}=\frac{c_0-\frac{2}{3}-c_1\xi-\left(c_2-\frac{2}{3}\right)\xi^2}{(1-\xi^2)^2},$$

We get

$$\psi''-\frac{2\xi}{1-\xi^2}\psi'+\frac{c_0-\frac{2}{3}-c_1\xi-\left(c_2-\frac{2}{3}\right)\xi^2}{1-\xi^2}\psi=0. \tag{3.9}$$

To solve this equation exactly we can apply Nikiforov-Uvarov method [9], which can be applied to the following second order differential equations:

$$\psi''+\frac{\tilde{\tau}}{\sigma}\psi'+\frac{\tilde{\sigma}}{\sigma^2}\psi=0. \tag{3.10}$$

Here, it is assumed that σ and $\tilde{\sigma}$ are arbitrary polynomials of at most second degree and $\tilde{\tau}$ is an arbitrary polynomial of at most first degree. The following comparison allows to say that Nikiforov-Uvarov method is applicable to exact solution of eq.(3.9):

$$\tilde{\tau}=-2\xi,\quad \sigma=1-\xi^2,\quad \tilde{\sigma}=c_0-\frac{2}{3}-c_1\xi-\left(c_2-\frac{2}{3}\right)\xi^2 \tag{3.11}$$

We look for expression of ψ as:

$$\psi=\varphi(\xi)y,\qquad \text{where}\qquad \varphi=e^{\int\frac{\pi(\xi)}{\sigma(\xi)}d\xi}. \tag{3.12}$$

Via simple computations one finds that

$$\psi'=\frac{\pi}{\sigma}\varphi y+\varphi y',$$

$$\psi''=\frac{\pi'\sigma-\pi\sigma+\pi^2}{\sigma^2}\varphi y+\frac{2\pi}{\sigma}\varphi y'+\varphi y''.$$

Taking these computations into account in (3.9) leads to the equation for $y(\xi)$:

$$y''+\frac{2\pi+\tilde{\tau}}{\sigma}y'+\frac{\bar{\sigma}+\pi^2+\pi(\tilde{\tau}-\sigma')+\pi'\sigma}{\sigma^2}y=0, \tag{3.13}$$

where

$$\tau=2\pi+\tilde{\tau},\qquad \bar{\sigma}=\tilde{\sigma}+\pi^2+\pi(\tilde{\tau}-\sigma')+\pi'\sigma. \tag{3.14}$$

We can rewrite (3.13), as

$$y'' + \frac{\tau}{\sigma}y' + \frac{\bar{\sigma}}{\sigma^2}y = 0 \tag{3.15}$$

Assuming that

$$\bar{\sigma} = \lambda\sigma, \qquad \lambda = \text{const}, \qquad \mu = \lambda - \pi', \tag{3.16}$$

we have

$$\lambda\sigma = \tilde{\sigma} + \pi^2 + \pi(\tilde{\tau} - \sigma') + \pi'\sigma,$$

which requires to solve the following quadratic equation:

$$\pi^2 + (\tilde{\tau} - \sigma')\pi + \tilde{\sigma} - \mu\sigma = 0.$$

Taking into account:

$$\sigma' = -2\xi, \qquad \tilde{\tau} - \sigma' = 0,$$

we find that

$$\pi = \varepsilon_1\sqrt{\mu\sigma - \tilde{\sigma}} = \varepsilon_1\sqrt{\mu + \frac{2}{3} - c_0 + c_1\xi + \left(c_2 - \left(\mu + \frac{2}{3}\right)\right)\xi^2}, \qquad \varepsilon_1 = \pm 1. \tag{3.17}$$

After some computations:

$$\mu = \frac{c_2 + c_0 + \varepsilon_2\sqrt{(c_2 - c_0)^2 - c_1^2}}{2} - \frac{2}{3}, \ \varepsilon_2 = \pm 1, \tag{3.18}$$

$$c_2 - \left(\mu + \frac{2}{3}\right) = \frac{c_2 - c_0 - \varepsilon_2\sqrt{(c_2 - c_0)^2 - c_1^2}}{2} = \kappa. \tag{3.19}$$

Substituting (3.18) & (3.19) at (3.17), we obtain the following expressions for π, τ and λ:

$$\pi = \varepsilon_1\left(\sqrt{\kappa}\xi + \frac{c_1}{2\sqrt{\kappa}}\right), \tag{3.20}$$

$$\tau = 2\varepsilon_1\left(\sqrt{\kappa}\xi + \frac{c_1}{2\sqrt{\kappa}}\right) - 2\xi = 2\left(\varepsilon_1\sqrt{\kappa} - 1\right)\xi + \varepsilon_1\frac{c_1}{\sqrt{\kappa}}. \tag{3.21}$$

$$\lambda = \mu + \pi' = \frac{c_2 + c_0 + \varepsilon_2\sqrt{(c_2 - c_0)^2 - c_1^2}}{2} - \frac{2}{3} + \varepsilon_1\sqrt{\kappa}. \tag{3.22}$$

Taking into account (3.20) at (3.12) we have to compute the following integral

$$\varphi(\xi) = e^{\int\frac{\pi(\xi)}{\sigma(\xi)}d\xi} = e^{\varepsilon_1\sqrt{\kappa}\int\frac{\xi}{1-\xi^2}d\xi}e^{\varepsilon_1\frac{c_1}{2\sqrt{\kappa}}\int\frac{1}{1-\xi^2}d\xi},$$

that gives for us

$$\varphi(\xi) = (1-\xi)^{-\kappa_1}(1+\xi)^{-\kappa_2},$$

$$\kappa_{1,2} = \frac{1}{2}\varepsilon_1\left(\sqrt{\kappa} \pm \frac{c_1}{2\sqrt{\kappa}}\right).$$

Finiteness of the $\varphi(\xi)$ at singular points $\xi = \pm 1$, i. e. the condition $\lim_{\xi\to\pm 1}\varphi(\xi) = const$ leads to

$$\varepsilon_1 = \varepsilon_2 = -1, \qquad \kappa > 0, \quad \kappa_{1,2} \le 0.$$

Therefore, we have

$$\mu = \frac{c_2 + c_0 - \sqrt{(c_2 - c_0)^2 - c_1^2}}{2} - \frac{2}{3}, \tag{3.23}$$

$$\pi = -\sqrt{\kappa}\xi - \frac{c_1}{2\sqrt{\kappa}}, \tag{3.24}$$

$$\kappa = \frac{c_2 - c_0 + \sqrt{(c_2 - c_0)^2 - c_1^2}}{2}, \tag{3.25}$$

$$\sqrt{\kappa} = -\kappa_1 - \kappa_2, \tag{3.26}$$

$$\kappa_{1,2} = -\frac{1}{2}\left(\sqrt{\kappa} \pm \frac{c_1}{2\sqrt{\kappa}}\right). \tag{3.27}$$

Then, expression of the wavefunction ψ also will have the following exact expression:

$$\psi = \varphi(\xi)y = (1-\xi)^{-\kappa_1}(1+\xi)^{-\kappa_2}y. \tag{3.28}$$

We also obtain the following expressions for $\pi(\xi)$, τ and λ in terms of κ_1 and κ_2:

$$\pi = (\kappa_1 + \kappa_2)\xi + \frac{c_1}{2(\kappa_1+\kappa_2)}, \quad (3.29)$$

$$\tau = 2(\kappa_1 + \kappa_2 - 1)\xi + \frac{c_1}{\kappa_1+\kappa_2}, \quad (3.30)$$

$$\lambda = \frac{c_2+c_0-\sqrt{(c_2-c_0)^2-c_1^2}}{2} - \frac{2}{3} + \kappa_1 + \kappa_2 . \quad (3.31)$$

Then, eq. (3.15) will have the form as follows:

$$\sigma y'' + \tau y' + \lambda y = 0. \quad (3.32)$$

Function $y(\xi)$ should be finite at values $\xi = \pm 1$. Therefore, we have to find its polynomial solutions. For this reason, we compare the following exact expression of eq. (3.32)

$$(1-\xi^2)y'' + \left[2(\kappa_1 + \kappa_2 - 1)\xi + \frac{c_1}{\kappa_1 + \kappa_2}\right]y' + \lambda y = 0$$

with the following second order differential equation for the Jacobi polynomials

$$(1-x^2)\bar{y}'' + [\beta - \alpha - (\alpha + \beta + 2)x]\bar{y}' + n(n + \alpha + \beta + 1)\bar{y} = 0,$$

where, $\bar{y} = P_n^{(\alpha,\beta)}(x)$ are Jacobi polynomials defined in terms of the ${}_2F_1$ hypergeometric functions as follows:

$$P_n^{(\alpha,\beta)}(x) = \frac{(\alpha+1)_n}{n!}\,{}_2F_1\left(\begin{matrix}-n, n+\alpha+\beta+1 \\ \alpha+1\end{matrix};\ \frac{1-x}{2}\right), \quad \alpha;\beta \neq -1/2,$$

$$\alpha + \beta = -2(\kappa_1 + \kappa_2),$$

$$\alpha + \beta = \frac{c_1}{\kappa_1+\kappa_2}.$$

Some computations lead us to the following non-equidistant energy spectrum:

$$E \equiv E_n^{gGI} = \hbar\omega\sqrt{\frac{1}{2} + \sqrt{\frac{1}{4} - \frac{g^2}{a^2\omega^4}}}\left(n + \frac{1}{2}\right) + \frac{\hbar^2}{2m_0a^2}n(n+1) + \frac{\hbar^2}{3m_0a^2} - $$
$$- m_0\omega^2a^2\left(\frac{1}{2} - \sqrt{\frac{1}{4} - \frac{g^2}{a^2\omega^4}}\right). \quad (3.33)$$

Wavefunctions of the stationary states have form:

$$\psi \equiv \psi_n^{gGI}(x) = c_n^{gL}\left(1 - \frac{x}{a}\right)^{-\kappa_1}\left(1 + \frac{x}{a}\right)^{-\kappa_2} P_n^{(-2\kappa_1,-2\kappa_2)}\left(\frac{x}{a}\right). \quad (3.34)$$

The normalization factor c_n^{gGI}

$$c_n^{gGI} = \frac{1}{2^{\sqrt{\kappa}+\frac{1}{2}}}\sqrt{\frac{(2n+2\sqrt{\kappa}+1)\Gamma(n+2\sqrt{\kappa}+1)n!}{a\Gamma(n-2\kappa_1+1)\Gamma(n-2\kappa_2+1)}} \quad (3.35)$$

is defined from the orthogonality relation for Jacobi polynomials $P_n^{(\alpha,\beta)}(x)$ of the following form

$$\int_{-1}^{1}(1-x)^\alpha(1+x)^\beta P_m^{(\alpha,\beta)}(x)\,P_n^{(\alpha,\beta)}(x)dx = \frac{2^{\alpha+\beta+1}}{2n+\alpha+\beta+1}\frac{\Gamma(n+\alpha+1)\Gamma(n+\beta+1)}{\Gamma(n+\alpha+\beta+1)n!}\delta_{mn},$$

within conditions $\alpha > -1$ and $\beta > -1$. Therefore, wavefunctions of the stationary states in the position representation are also orthogonal in the finite region $-a < x < a$:

$$\int_{-a}^{a}\left[\psi_m^{gGI}(x)\right]^*\psi_n^{gGI}(x)dx = \delta_{mn}.$$

Thanks to analytical expressions of energy spectrum (3.33) and wavefunctions (3.34) obtained via exact solution of the Schrödinger equation (3.9), we achieved our main goal. Now, we will discuss briefly some limit relations and special cases of these results in final section of the paper.

4. DISCUSSIONS AND LIMIT RELATIONS

Let's discuss obtained expressions for the energy spectrum (3.33) and wavefunctions of the stationary states (3.34) of a confined position-dependent mass harmonic oscillator.

It is clear that both energy spectrum (3.33) and wavefunctions of the stationary states (3.34) easily recover energy spectrum (3.5) and wavefunctions of the stationary states (3.6) in case of $g = 0$. They also recover energy spectrum (2.14) and wavefunctions of the stationary states (2.15) of the nonrelativistic quantum harmonic oscillator, if $a \to \infty$. It proves the correctness of our computations. Here, one needs to take into account two important results of the mathematics – first one is a Taylor expansion of the square root and second one special case relation between the Jacobi and Gegenbauer polynomials.

Our conclusion is that the model considered here is interesting and its behavior cordially differs from behavior of the ordinary harmonic oscillator under the external gravitational field. Confinement effects and unique non-linear picture of the energy spectrum appeared here can extend its potential applications in future.

[1] *O. Von Roos.* "Position-dependent effective mass in semiconductor theory", Phys. Rev., B 27, 1983, 7547.

[2] *D.L. Smith, C. Mailhiot.* "Theory of semiconductor superlattice electronic structure", Rev. Mod. Phys. 62, 1990, 173.

[3] *M. Pi, S.M. Gatica, E.S. Hernandez and J. Navarro.* "Structure and energetics of mixed 4 He-3 He drops", Phys. Rev. B 56, 1997, 8997.

[4] *G.T. Einevoll.* "Operator ordering in effective mass theory for heterostructures II. Strained systems", Phys. Rev. B 42, 1990, 3497.

[5] *A.D. Alhaidari.* "Solution of the Dirac equation with position-dependent mass in the Coulomb field", Phys. Lett. A, 322, 2004, 72–77.

[6] *S.M. Nagiyev and K.S. Jafarova.* "Relativistic quantum particle in a time-dependent homogeneous field", Phys. Lett. A, 377, 2013, 747–752.

[7] *E.I. Jafarov and A.M. Mammadova.* "On the exact solution of the confined position-dependent mass harmonic oscillator model under the kinetic energy operator compatible with Galilean invariance". Azerb. J. Phys. - Fizika, 26, 2020, 31-35.

[8] *R.F. Lima, M. Vieira, C. Furtado, F. Moraes and Cleverson Filgueiras.* "Yet another position-dependent mass quantum model". J. Math. Phys., 53, 2012, 072101.

[9] *A.F. Nikiforov and V.B. Uvarov.* Special Functions of Mathematical Physics (Birkhauser, Basel, 1988).

Received: 30.09.2021

ISSN 1028-8546

2021, Vol. XXVII, № 3
Section: En

CONTENTS